Miner Petrol (2013) 107:829–848
DOI 10.1007/s00710-012-0204-z

SPECIAL ISSUE GONDWANA COLLISION

Neoproterozoic ophiolitic peridotites along the Allaqi-Heiani suture, South Eastern Desert, Egypt

M. K. Azer · M. D. Samuel · K. A. Ali · H. A. Gahlan · R. J. Stern · M. Ren · H. E. Moussa

Received: 1 June 2011 / Accepted: 17 May 2012 / Published online: 8 June 2012

Abstract The Wadi Allaqi ophiolite along the Egyptian-Sudanese border defines the southernmost ophiolitic assemblage and suture zone in the Eastern Desert. Ophiolite assemblages comprise nappes composed mainly of mafic and ultramafic rocks that were tectonically emplaced and replaced by serpentine and carbonates along shear zones probably due to CO_2-metasomatism. Serpentinites, altered slices of the upper mantle, represent a distinctive lithology of dismembered ophiolites of the western YOSHGAH suture. Microscopically, they are composed of more than 90 % serpentine minerals with minor opaque minerals, carbonate, brucite and talc. The mineral chemistry and whole-rock chemical data reported here indicate that the serpentinized peridotites formed as highly-depleted mantle residues. They show compositions consistent with formation in a suprasubduction zone environment. They are depleted in Al_2O_3 and CaO similar to those in fore-arc peridotites. Also, high Cr# (Cr/ (Cr+Al)) in the relict chrome spinels (average ~0.72) indicates that these are residual after extensive partial melting, similar to spinels in modern fore-arc peridotites. Therefore, the studied serpentinites represent fragments of an oceanic lithosphere that formed in a fore-arc environment, which belongs to an ophiolitic mantle sequence formed in a suprasubduction zone.

Editorial handling: K. Stüwe

M. K. Azer (✉) · M. D. Samuel · H. E. Moussa
Geology Department, National Research Centre,
12622-Dokki,
Cairo, Egypt
e-mail: mokhles72@yahoo.com

K. A. Ali
Department of Mineral Resources and Rocks, Faculty of Earth Sciences, King Abdulaziz University,
P.O. Box 80206, Jeddah 21589, Saudi Arabia

R. J. Stern
Geosciences Department, University of Texas at Dallas,
800 W Campbell Rd.,
Richardson, TX 75080, USA

H. A. Gahlan
Geology Department, Assiut University, Faculty of Science,
Assiut 71516, Egypt

M. Ren
Department of Geological Sciences, University of Texas at El Paso,
El Paso, TX, USA

Introduction

The Arabian–Nubian Shield (ANS) is a large (~1,000,000 km^2) tract of juvenile crust that formed by terrane accretion during the Neoproterozoic era between major fragments of E and W Gondwana (Stern 2002; Johnson and Woldehaimanot 2003). Ophiolites are key components of the ANS, defining sutures and the location of fossil subduction zones as well as providing important clues about tectonic setting and hosting ore deposits (Price 1984; Pallister et al. 1988; Berhe 1990; Stern et al. 2003; Dilek and Ahmed 2003). Nevertheless, the significance of ANS ophiolites is controversial, partly because they are variably dismembered, deformed, and altered and partly because many have not been studied, especially ophiolites in southern Egypt and NE Sudan. These complications are particularly severe for serpentinized ultramafics, which are the single most distinctive lithology of dismembered ANS ophiolites and mélanges. The Neoproterozoic ophiolites of the ANS are documented from Egypt, Sudan and Saudi Arabia and are suspected to exist in Eritrea, Ethiopia, and Kenya. The ANS ophiolites range in age from 694±8 Ma to 870±11 Ma with a mean age of 781 Ma (Stern et al. 2003). Ophiolite formation and emplacement was clearly a key aspect of Cryogenian development of the ANS and Neoproterozoic formation of the Greater Gondwana supercontinent.

Neoproterozoic ophiolites and ophiolitic mélange are common in the central and southern sectors of the Eastern Desert of Egypt (Fig. 1). In a few places (e.g., Fawkhir, Ghadir, Gerf) a complete ophiolite stratigraphy can be seen, including a lower, mantle sequence of serpentinized ultramafics and an upper crustal sequence of layered and isotropic gabbros, sheeted dykes and mafic lavas including pillow basalts. Mostly the Egyptian ophiolites occur as tectonized bodies and mélanges of these ophiolitic lithologies (El Sharkawy and El Bayoumi 1979). Because of folding and shearing, most Egyptian ophiolites lack one or more of these diagnostic lithologies, but ophiolitic mélange is inferred wherever abundant serpentinite and metabasalt is juxtaposed. Most Egyptian ophiolites have been metamorphosed to low-grade greenschist facies, but in places the rocks reach amphibolite grade. Ophiolitic peridotites were altered by large volumes of fluids of diverse composition, resulting in serpentinization, silicification and carbonatization (e.g. Stern and Gwinn 1990; Azer 2008). Alteration resulted in the development of listwaenite, particularly in shear zones, and locally the only evidence that ophiolitic rocks underlie a given area is the presence of erosion-resistant listwaenite ridges.

Our understanding of ophiolites and ophiolitic peridotites in the Central Eastern Desert is rapidly improving (e.g. El Sayed et al. 1999; Ahmed et al. 2001; Farahat et al. 2004; Azer and Khalil 2005; Ahmed et al. 2006; Azer and Stern 2007; Khalil and Azer 2007; Farahat 2008; Abd El-Rahman et al. 2009a, b; Abu El Ela and Farahat 2010; Basta et al. 2011). Much less progress has been made understanding ophiolites of the less accessible South Eastern Desert. This is particularly unfortunate because this region hosts the only true suture zone in Egypt, the Allaqi-Heiani-Gerf ophiolite belt. This is the westernmost part of the Ess-Yanbu-Onib-Sol Hamed-Gerf-Allaqi-Heiani belt (YOSHGAH suture) which trends from the western edge of the northern Arabian Shield to Lake Nasser. Few petrologic studies are available about the ophiolitic rocks of this belt (Zimmer et al. 1995; Noweir et al. 2007; Gahlan and Arai 2009; Ali et al. 2010; Azer 2012), and detailed geological, petrographical and geochemical studies are scarce.

An important aspect of the present study is a focus on ophiolitic peridotites. In the past, studies of the Egyptian ophiolites have focused on volcanic rocks for evaluating their tectonic setting and petrogenesis. Mantle peridotites provide complementary information about petrogenesis and tectonic setting but the Egyptian ophiolitic peridotites have been largely ignored until recently (El Bahariya and Arai 2003; Azer and Khalil 2005; Azer and Stern 2007; Khalil and Azer 2007; Farahat 2008). In particular, there are no modern studies of ophiolitic ultramafic rocks of the Allaqi-Heiani-Gerf ophiolites west of G. Gerf (Zimmer et al. 1995).

This contribution reports the results of the first study of the geology, petrology, mineral chemistry and geochemistry of ophiolitic ultramafic rocks from the westernmost Allaqi-Heiani suture. We use these results to interpret the origin and tectonic setting of the Allaqi-Heiani-Gerf ophiolite. We hope this work encourages other researchers to begin studying ophiolites in this region; accordingly the significance of these rocks in the evolution of the ANS and its mineralization can be better assessed.

Regional geology

Mafic-ultramafic rocks constitute one of the distinctive rock units in the Egyptian basement. They comprise about 5 % of all Precambrian outcrops in the Eastern Desert of Egypt (Dixon 1979). The Egyptian Neoproterozoic mafic-ultramafic complexes are divided into two main groups based on their lithostratigraphic position; ophiolites and intrusions. The ophiolites are generally dismembered, representing remnants of oceanic lithosphere that coexisted with the ANS Neoproterozoic intra-oceanic arcs. The ages of Eastern Desert ophiolites range from ~737 to ~720 Ma (Kröner et al. 1992; Zimmer et al. 1995; Loizenbauer et al. 2001; Andresen et al. 2009; Ali et al. 2010). Ophiolitic ultramafics are easily distinguished from intrusive mafic-ultramafic bodies because the latter form undeformed small, elliptical outcrops and are commonly concentrically zoned or layered and undeformed (Helmy and El Mahallawi 2003; Farahat and Helmy 2006; Azer and El-Gharbawy 2011). The zoned mafic-ultramafic complexes are considered as Precambrian analogues of Alaskan-type complexes and may represent the roots of arc volcanoes (Dixon 1981a; Helmy and El Mahallawi 2003; Farahat and Helmy 2006). Only the Dahanib complex has been dated, which has a conventional U-Pb zircon age of 711±7 Ma (Dixon 1981b).

Most South Eastern Desert ophiolites are found along the Allaqi-Heiani-Gerf suture zone, which can be traced for ~400 km from Lake Nasser to the Red Sea. This is the western part of a much longer ophiolite-decorated suture zone, the Ess-Yanbu-Onib-Sol Hamed-Gerf-Allaqi-Heiani belt (YOSHGAH suture of Stern et al. 1990) which trends from the western edge of the northern Arabian Shield to Lake Nasser. The YOSHGAH suture is considered – along with the Ariab-Nakasib-Thurwah-Bir Umq suture farther south in Arabia and Sudan (Johnson et al. 2004) to be one of the two longest and most complete Neoproterozoic ophiolite-decorated sutures in the ANS. With the Red Sea closed, the YOSHGAH ophiolite belt can be traced ~600 km across the Nubian and Arabian shields. This suture formed by the collision of the South Eastern Desert (Gerf)-Midyan terrane to the north with the Gebeit terrane to the south (Kröner et al. 1987) and is decorated by variably disrupted ophiolite fragments. Ali et al. (2010) suggested two stages for the evolution of YOSHGAH ophiolite belt (~810–

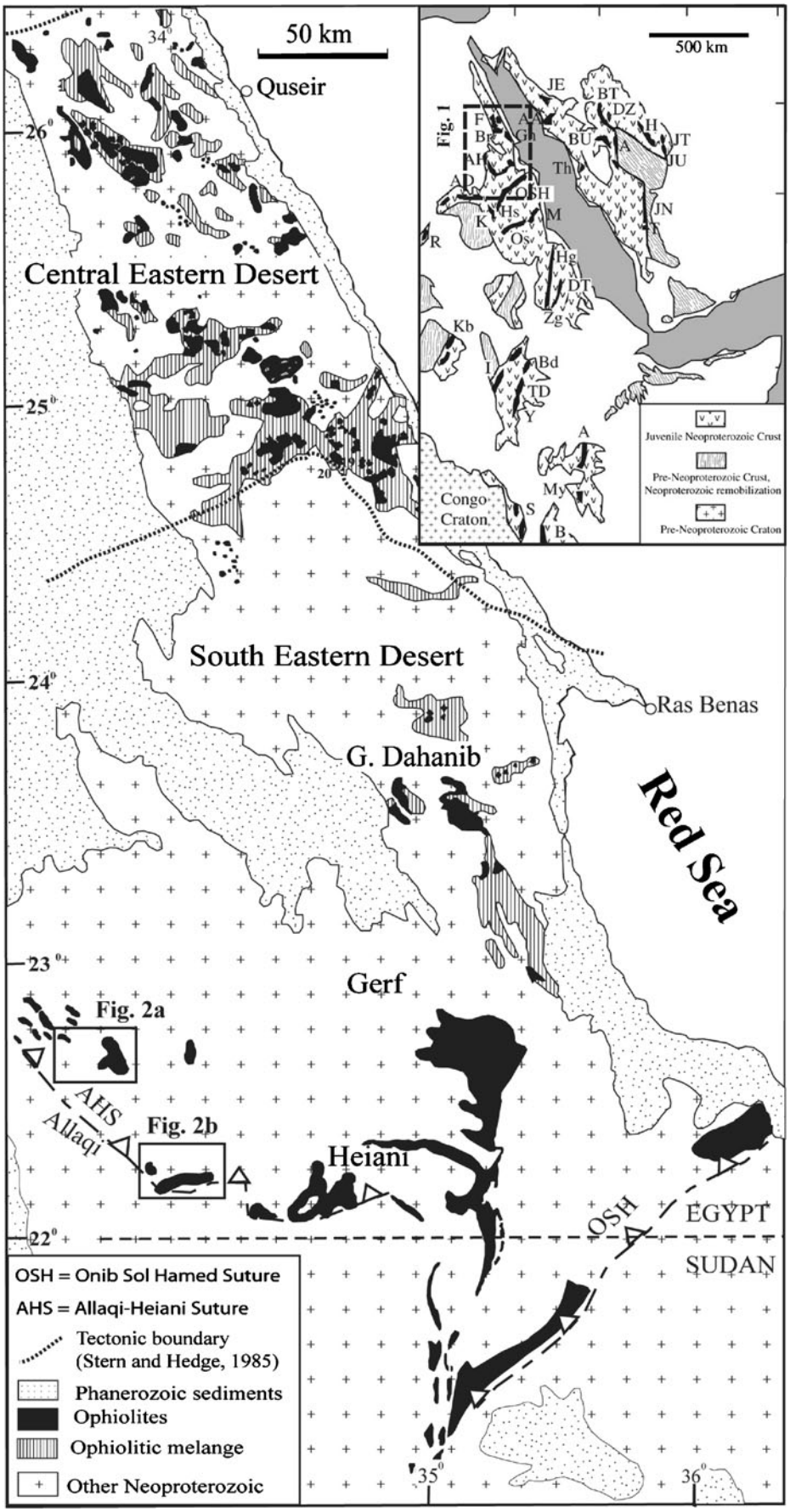

Fig. 1 Distribution of ophiolitic rocks in Eastern Desert of Egypt (modified after Shackleton 1994). The location of Fig. 2a and b is indicated. Inset shows the location of the Eastern Desert in the northernmost ANS Neoproterozoic exposures and the location of Fig. 1 is indicated (Stern et al. 2004)

780 Ma and ~750–730 Ma). They concluded that accretion between the Gabgaba-Gebeit-Hijaz terranes to the south and the South Eastern Desert-Midyan terranes to the north occurred as early as 730 Ma and no later than 709±4 Ma.

A major E-W drainage, Wadi Allaqi, follows the YOSHGAH suture zone structural trends, which is defined by the curvilinear ophiolitic belt that can be traced for more than 200 km across the Egyptian shield west of the Hamisana Shear Zone, near the border with Sudan (Kröner et al. 1987). The Allaqi suture zone is broad and comprises gneiss, dismembered ophiolites, island arc volcanosedimentary-plutonic assemblages, and syn- to post-orogenic intrusions (e.g. Kröner et al. 1987; Greiling et al. 1988; Taylor et al. 1993; Abd El-Naby and Frisch 2002; Kusky and Ramadan 2002; Abdelsalam et al. 2003; Zoheir and Klemm 2007; Ali et al. 2010). The dismembered ophiolite assemblages comprise nappes composed mainly of mafic and ultramafic rocks and their alteration products. The serpentinites represent a distinctive lithology of dismembered ophiolites of the western YOSHGAH suture. Some portions contain relicts of primary minerals and others are extremely altered, especially along thrusts and shear zones, with the development of talc, talc-carbonate and reddish brown quartz-carbonate rock (listwaenite). Stern et al. (1990) inferred that the Allaqi-Heiani ophiolitic nappe verged south during emplacement, and was then shortened E-W, most importantly in the region along the N-S Hamisana Shear Zone (de Wall et al. 2001), during terminal collision between E and W Gondwana at ~630 Ma. Kusky and Ramadan (2002) suggested that the Allaqi-Heiani suture is an arc/arc collision zone, formed when the Gerf terrane overrode the Gabgaba terrane prior to closure of the Mozambique Ocean. This suture hosts important mineral deposits, such as gold, chromite, magnesite and talc (Klemm et al. 2001; Kusky and Ramadan 2002; Oweiss et al. 2001; Zoheir 2008; Azer 2012).

Field description

The present study concentrated on two localities (Fig. 2a, b) along the Wadi Allaqi suture, from W to E: Jabal Shilman and Jabal Moqsim.

Jabal Shilman area

Basement rocks around Jabal Shilman include immature metasediments, dismembered ophiolitic rocks, island arc-related assemblages, and syn- to post-orogenic granitoids (Fig. 2a). Dismembered ophiolitic rocks of Jabal Shilman define the northwestern continuation of the Allaqi-Heiani ophiolite belt (Kröner et al. 1987). They are overlain by the arc metavolcanic–metasedimentary succession (Fig. 3a) and intruded by syn- to post-tectonic granitoids. The dismembered ophiolitic rocks include completely serpentinized peridotites and talc carbonates as well as metagabbros. The largest serpentinite mass occurs at Jabal Shilman, which is also associated with a large metagabbro mass (Fig. 3b). Another small serpentinite masses occur at north-west as well as north-east corners of the mapped area and are associated with marble and listwaenite. Field relationships of serpentinites with most other rock units are concealed by sand and wadis fill. The serpentinites are altered to listwaenite along contacts with the volcano-sedimentary rocks and granodiorites. The listwaenites form ridges due to their resistance against weathering relative to the surrounding rocks (Fig. 3c; adopted from Azer 2012). Metasediments are represented by gneiss and marble.

There are some age constraints for the basement rocks of the Jabal Shilman area. Kröner et al. (1992) obtained single zircon Pb-Pb evaporation ages of 729±17 Ma and 736±11 Ma for metagabbro and metadiorite associated with serpentinites, respectively. Arc metavolcanics are represented mainly by meta-andesite and metadacite; a sample of the latter gave a U-Pb zircon SHRIMP age of 733±7 Ma (Ali et al. 2010). Syn-tectonic granitoids include granodiorite, interpreted as arc-related and I-type (El-Kazzaz and Taylor 2001) gave a U-Pb zircon SHRIMP age of 629±5 Ma (Ali et al. 2010), while a post-tectonic granite, one of several such plutons in the region (El-Kazzaz and Taylor 2001), gave a U-Pb zircon SHRIMP age of 603±14 Ma (Moussa et al. 2008).

Jabal Moqsim area

Basement rocks in Jabal Moqsim area comprise dismembered ophiolitic rocks, island arc-related assemblages, and syn-orogenic intrusions (Fig. 2b). The mafic-ultramafic suite of Wadi Abu Fas, to the west of Jabal Moqsim, is one of the largest mafic-ultramafic occurrences in the south Eastern Desert (~ 75 km^2) and was considered to be an arc-related layered intrusion (Sadek and El-Ramly 1996). The layered gabbros of Wadi Abu Fas are considered as ophiolitic gabbro and gave a U-Pb zircon SHRIMP age of 730±6 Ma (Ali et al. 2010).

Most of the dismembered ophiolitic rocks of Jabal Moqsim consist of serpentinite and talc-carbonate as well as a small (~50 m diameter) body of gabbro, which appears to intrude the serpentinite. The serpentinites occupy large areas and form conspicuous mountainous ridges with steep slopes. They are generally massive, but locally affected by shear zones. Foliation of the intensively sheared serpentinites is parallel to the schistosity of the surrounding metavolcanic rocks. Along shear zones, the serpentinite bodies are replaced by talc-carbonates due to CO_2 metasomatism (Fig. 3d). Ali et al. (2010) obtained an age of 697±5 Ma for the small gabbroic mass of Jabal Moqsim, representing the

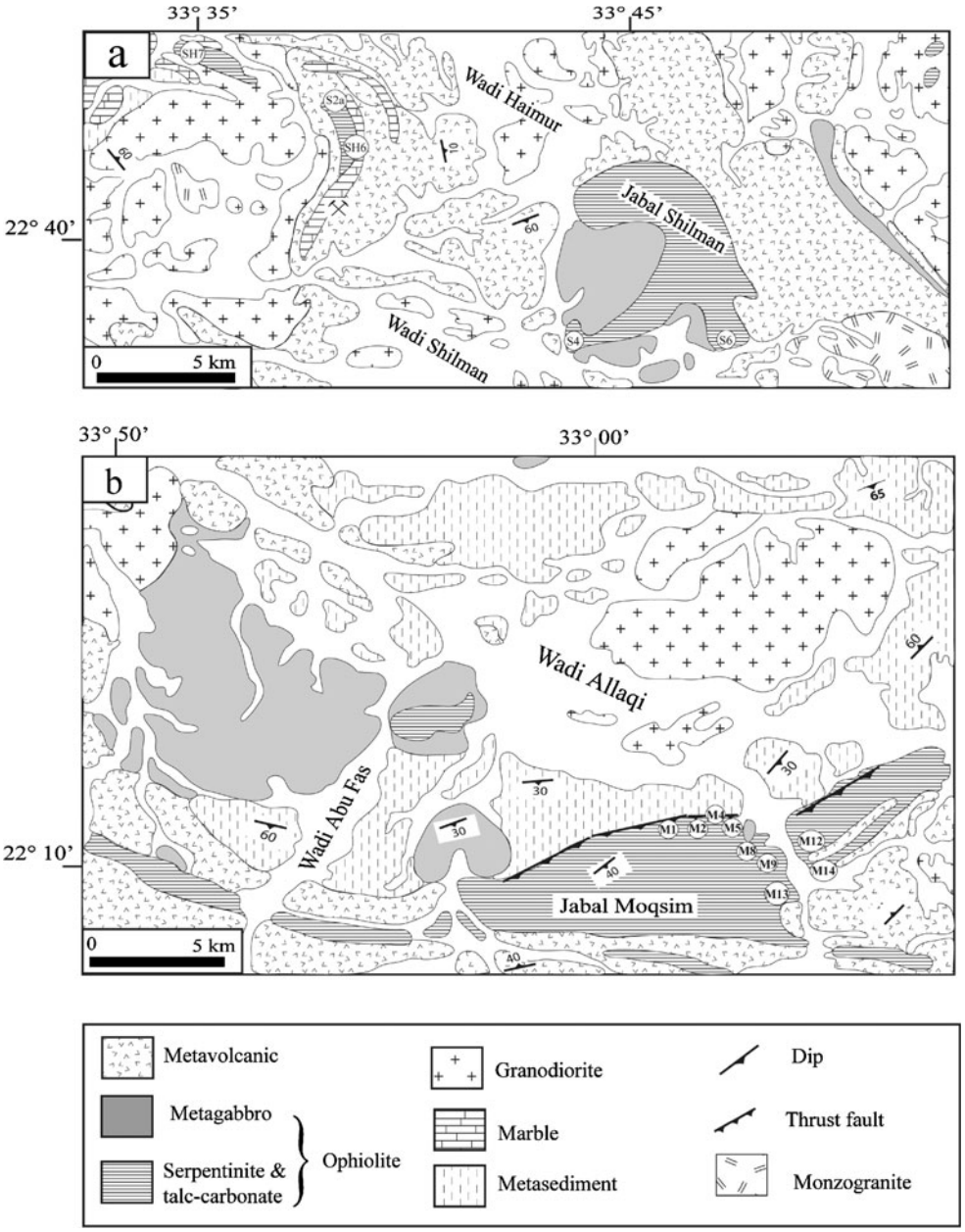

Fig. 2 Detailed geological maps of the study areas (after Ali et al. 2010), showing the sample locations; **a** Jabal Shilman area and **b** Jabal Moqsim area

age of intrusion and crystallization of the gabbro into the already sheared serpentinite of the ophiolite. Arc metavolcanic rocks in the Jabal Moqsim area are metamorphosed to greenschist facies (El-Nisr 1997). Metasediments consist of marble, schist, greywacke and subordinate conglomerate (El Gaby et al. 1988).

Analytical techniques

Some serpentinite samples were subjected to X-ray powder diffraction (XRD) analysis to determine their mineralogical composition. The powder diffraction pattern of the samples was obtained with Cu radiation with secondary monochrometer. The scanning speed was 2 h=1 deg/min at constant voltage 40 kV and 40 mA using BRUKUR D8 advanced X-ray diffractometer at the Central Metallurgical and Development Institute in Cairo, Egypt. Mineral identification was carried out using the data given in the American Standard Test Materials (ASTM) cards by measuring the d-values of the different atomic planes and their relative intensities.

Mineral chemical analyses were performed by electron probe microanalysis (EPMA) on a Cameca SX50 instrument under operating condition of 15 kV accelerating voltage, 20 nA beam current, 5–10 μm beam size, and 20 s peak counting time. Suitable synthetic and natural mineral standards were applied for calibration. The mineral chemical analyses were carried at the University of Texas at El Paso, U.S.A.

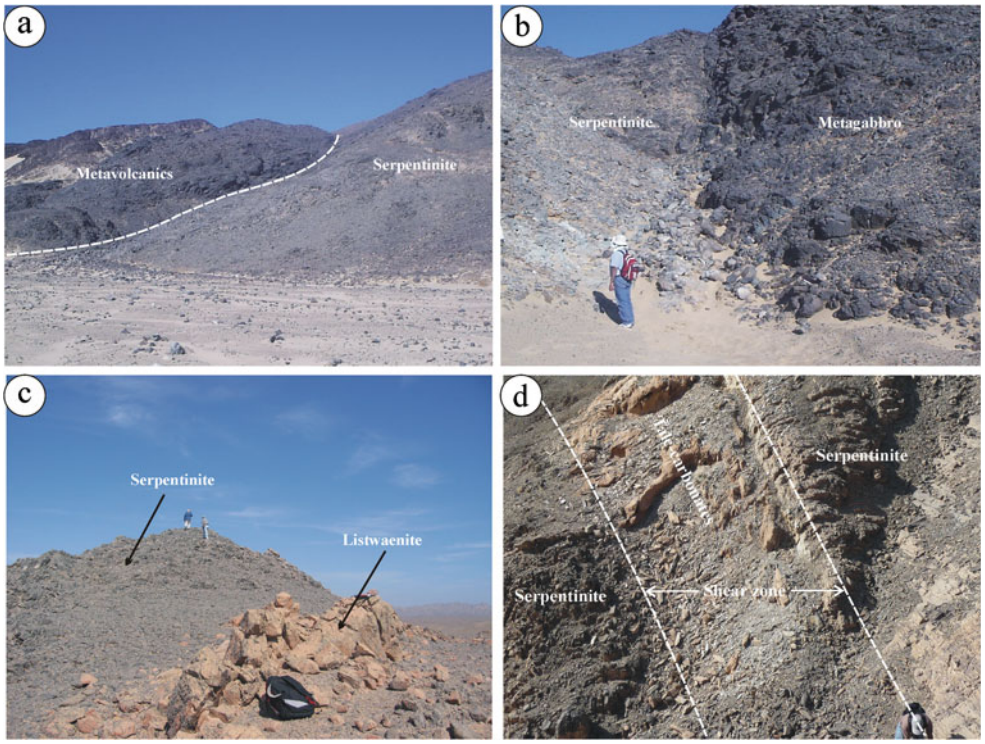

Fig. 3 **a** Ophiolitic rocks of Jabal Shilman are overlain by arc metavolcanics, **b** Sharp contact between serpentinite and metagabbro at Jabal Shilman, **c** Listwaenite ridge associated with serpentinite in Jabal Shilman area, and **d** Serpentinite is replaced by talc-carbonate rocks along shear zones at Jabal Moqsim

Powders were prepared for analysis at the University of Texas at Dallas (UTD) and analyzed for major and selected trace elements (Ba, Sr, Y, Sc, Zr, Be, and V) using fusion-ICP-MS whole rock techniques at ACTLABS, Canada (Table 6).

Petrographic description

Jabal Shilman

Dismembered ophiolitic rocks of Jabal Shilman are mainly ultramafics and metagabbros. The ultramafic rocks are fine- to medium-grained with dark green or greenish black color and are completely serpentinized. Microscopically, serpentinites composed of more than 90 % serpentine minerals with minor opaque minerals, carbonate, brucite and talc. Sometimes, the serpentine minerals retain the geometric configuration of the original mafic minerals; serpentine developed as an alteration after olivine has a mesh texture while that formed after orthopyroxene has a bastite texture. These textures indicate dunite and harzburgite parent rocks. The serpentine minerals are mainly antigorite with subordinate lizardite. Antigorite occurs as irregular aggregates composed of lamellar, platy or fibrous aggregate crystals display flame-texture. Lizardite is mostly subordinate and interstitial between antigorite. It occurs as elongated crystals having fibrous habit and sometimes agglomerated to give a bundle-like texture. Opaque minerals are magnetite and minor pyrite. Disseminated chromite is common in serpentinites and occurs as subhedral to euhedral crystals (Fig. 4a) colored a characteristic reddish brown. Chromite is typically unaltered but may have rims of ferritchromite and magnetite (Fig. 4b) due to regional metamorphism. Carbonates are magnesite and dolomite. Magnesite occurs as sparse crystals and fine aggregates in the massive serpentinites or as veinlets and pockets in the sheared varieties. The magnesite veinlets are monomineralic and cryptocrystalline with sharp contacts with the enclosing serpentinites. Brucite appears as platy or fibrous crystals intermixed with serpentines.

Metagabbros composed essentially of actinolite, plagioclase, subordinate clinopyroxene and opaque minerals. They show a characteristic ophitic-subophitic texture. Plagioclase occurs as large poikilitic plates replaced completely by intergrown albite and epidote. Apatite and zircon are the main accessories. Actinolite occurs as light green laths and/or aggregates replacing partly or completely clinopyroxene.

Jabal Moqsim

Dismembered ophiolitic rocks of Jabal Moqsim are mainly serpentinites with a small mass of metagabbro and talc-carbonates. The serpentinites are composed mainly of antigorite and subordinate chrysotile with minor carbonate, brucite and opaque minerals. Generally, the serpentinites exhibit bastite and mesh textures. They commonly show a

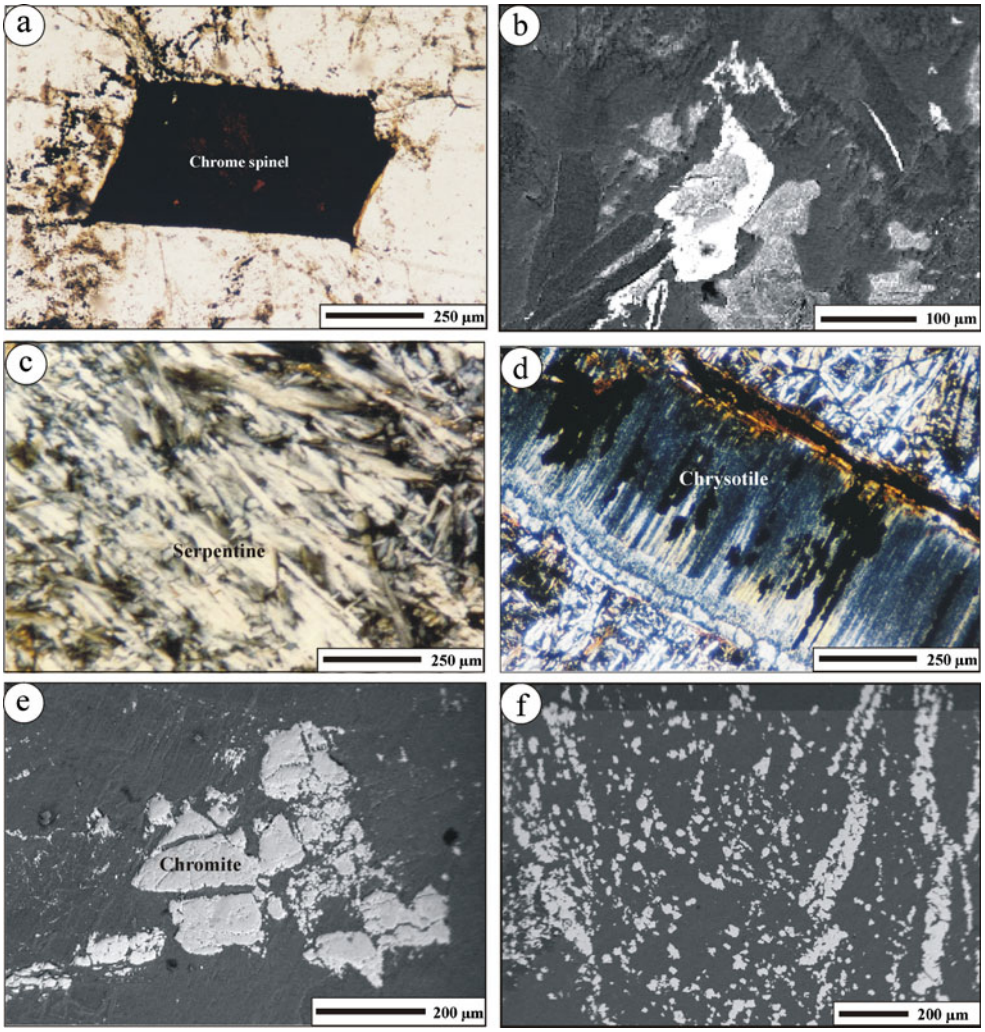

Fig. 4 **a** Euhedral disseminated chrome spinels in the serpentinites of Jabal Shilman (plane-polarized light), **b** Back-scattered electron image showing replacement of chrome-spinel (dark gray area) by Fe-rich spinel (light gray area) during regional metamorphism, **c** Serpentine minerals exhibit preferred orientation (cross-polarized light), **d** Chrysotile occurs as cross-fiber veinlets traversing the antigorite matrix in the serpentinites of Jabal Moqsim (cross-polarized light), **e** Back-scattered electron image showing characteristic cataclastic texture in the chromite along shear zone, and **f** Back-scattered electron image showing secondary magnetite as both fine dusty magnetite and stringers of small discontinuous veinlets

somewhat preferred orientation (Fig. 4c). Where crystals are aligned in two directions, most of them trend in one direction, which may indicate changing stress direction. Antigorite occurs as irregular masses composed of lamellar, platy or fibrous aggregates that frequently display flame-like texture. Chrysotile occurs as cross-fiber veinlets traversing the antigorite matrix (Fig. 4d). Carbonate minerals are mainly magnesite which occurs as fine rounded to anhedral crystals. Disseminated chromite occurs as ellipsoidal and elongated grains with a characteristic reddish brown or dark brown color. Along shear zones, chromite crystals show a characteristic cataclastic texture (Fig. 4e), and are replaced by ferritchromite and magnetite. Opaque minerals are mainly magnetite, pyrite and minor chalcopyrite. Magnetite is secondary after alteration of spinel, olivine and pyroxenes. It occurs as both fine dusty magnetite and stringers of small discontinuous veinlets (Fig. 4f). Brucite occurs as fibrous crystals intermixed with serpentines.

Metagabbros are coarse-grained and consist of highly-altered crystals of plagioclase, clinopyroxene (altered to actinolite), amphibole and accessory apatite, Fe-oxides and zircon. Talc-carbonates are fine grained and foliated. They composed mainly of magnesite, talc and less commonly serpentine minerals and chromite.

Mineral chemistry

The chemistry of preserved minerals, particularly olivine, spinel and pyroxene, reflects the magmatic conditions and the tectonic environment of the ultramafic parent rocks. Unfortunately the studied rocks are highly altered, and chromite is the only primary mineral preserved. Chemical compositions of serpentines, chrome spinels, magnetite and carbonates were determined by electron microprobe techniques.

Serpentine minerals

Representative chemical analyses of the serpentine minerals from Jabal Shilman and Jabal Moqsim serpentinites are listed in Tables 1 and 2. The composition of the analyzed serpentine minerals in the two localities is nearly similar.

Table 1 Microprobe analyses of serpentine minerals in serpentinites of Jabal Shilman

	S2a									S6												
	#1	#2	#3	#4	#5	#10	#12	#17	#18	#1	#2	#3	#4	#5	#6	#19	#20	#21	#26	#29	#30	#40
SiO_2	43.20	43.15	43.14	42.87	43.42	42.66	42.47	42.41	42.16	43.73	43.92	44.01	43.83	43.42	44.97	43.73	42.73	44.04	44.02	43.98	43.96	43.33
TiO_2	0.06	0.02	0.00	0.06	0.07	0.05	0.02	0.03	0.06	0.01	0.00	0.00	0.02	0.02	0.03	0.00	0.01	0.00	0.02	0.02	0.00	0.02
Al_2O_3	0.36	0.41	0.28	0.56	0.42	0.39	0.31	0.33	0.30	0.00	0.00	0.00	0.03	0.00	0.00	0.37	0.03	0.04	0.00	0.09	0.10	0.01
Cr_2O_3	0.00	0.02	0.06	0.62	0.51	0.26	0.27	0.02	0.19	0.02	0.01	0.03	0.03	0.04	0.02	0.10	0.05	0.01	0.05	0.05	0.05	0.06
FeO	1.78	1.74	1.98	1.86	1.76	1.89	1.88	1.91	1.93	1.23	1.53	2.27	1.42	1.49	4.35	7.21	6.72	2.12	5.08	7.33	7.13	3.98
MnO	0.00	0.00	0.00	0.02	0.00	0.00	0.02	0.02	0.00	0.00	0.00	0.00	0.00	0.00	0.00	0.02	0.07	0.01	0.04	0.11	0.12	0.00
MgO	40.28	39.99	40.54	39.46	39.49	38.98	39.55	39.93	39.86	41.06	41.40	41.22	41.50	41.49	38.41	37.06	37.94	40.33	38.79	36.51	37.15	38.86
CaO	0.04	0.04	0.05	0.08	0.11	0.09	0.07	0.02	0.04	0.01	0.03	0.04	0.03	0.01	0.07	0.03	0.08	0.10	0.19	0.02	0.02	0.10
Na_2O	0.01	0.00	0.01	0.01	0.00	0.01	0.00	0.00	0.00	0.01	0.03	0.02	0.02	0.00	0.01	0.02	0.02	0.01	0.02	0.00	0.01	0.01
K_2O	0.00	0.00	0.00	0.00	0.00	0.00	0.00	0.00	0.00	0.00	0.00	0.01	0.01	0.01	0.02	0.01	0.03	0.01	0.01	0.01	0.01	0.02
P_2O_5	0.00	0.00	0.00	0.00	0.00	0.00	0.00	0.00	0.00	0.04	0.00	0.01	0.05	0.05	0.06	0.03	0.05	0.01	0.04	0.06	0.05	0.04
Total	85.87	85.46	86.08	85.60	85.91	84.49	84.74	84.71	84.56	86.49	87.02	87.73	87.02	86.62	88.04	88.74	87.90	86.85	88.42	88.22	88.68	86.59
Si	2.032	2.038	2.027	2.027	2.042	2.042	2.029	2.024	2.018	2.042	2.037	2.033	2.031	2.024	2.083	2.044	2.019	2.051	2.045	2.065	2.055	2.045
Ti	0.002	0.001	0.000	0.002	0.003	0.002	0.001	0.001	0.002	0.000	0.000	0.000	0.001	0.001	0.001	0.000	0.000	0.000	0.001	0.001	0.000	0.001
Al	0.020	0.023	0.015	0.031	0.023	0.022	0.018	0.019	0.017	0.000	0.000	0.000	0.002	0.000	0.000	0.020	0.001	0.002	0.000	0.005	0.005	0.000
Cr	0.000	0.001	0.002	0.023	0.019	0.010	0.010	0.001	0.007	0.001	0.000	0.001	0.001	0.001	0.001	0.004	0.002	0.000	0.002	0.002	0.002	0.002
Fe	0.070	0.069	0.078	0.073	0.069	0.076	0.075	0.076	0.077	0.048	0.059	0.088	0.055	0.058	0.169	0.282	0.266	0.083	0.197	0.288	0.279	0.157
Mn	0.000	0.000	0.000	0.001	0.000	0.000	0.001	0.001	0.000	0.000	0.000	0.000	0.000	0.000	0.000	0.001	0.003	0.000	0.002	0.004	0.005	0.000
Mg	2.825	2.816	2.840	2.781	2.769	2.782	2.817	2.841	2.845	2.859	2.862	2.838	2.867	2.883	2.652	2.583	2.672	2.800	2.687	2.556	2.589	2.734
Ca	0.002	0.002	0.003	0.004	0.005	0.004	0.004	0.001	0.002	0.001	0.002	0.002	0.001	0.001	0.003	0.001	0.004	0.005	0.009	0.001	0.001	0.005
Na	0.001	0.000	0.001	0.001	0.000	0.001	0.000	0.000	0.000	0.001	0.003	0.001	0.002	0.000	0.001	0.002	0.002	0.001	0.002	0.000	0.000	0.001
K	0.000	0.000	0.000	0.000	0.000	0.000	0.000	0.000	0.000	0.000	0.000	0.000	0.001	0.000	0.001	0.001	0.002	0.001	0.001	0.001	0.001	0.001
P	0.000	0.000	0.000	0.000	0.000	0.000	0.000	0.000	0.000	0.002	0.000	0.001	0.002	0.002	0.002	0.001	0.002	0.001	0.002	0.002	0.002	0.002
Total	4.951	4.949	4.965	4.943	4.931	4.939	4.955	4.964	4.968	4.954	4.963	4.964	4.963	4.970	4.913	4.939	4.973	4.945	4.946	4.925	4.938	4.949

Table 2 Microprobe analyses of serpentine minerals in serpentinites of Jabal Moqsim

	M1													M2				
	#1	#2	#3	#4	#5	#6	#7	#9	#10	#21	#28	#29	#30	#2	#3	#4	#5	#6
SiO_2	43.52	43.36	43.46	43.74	42.90	43.17	42.34	42.97	43.06	43.53	44.76	44.29	43.77	45.06	45.01	44.81	44.97	44.88
TiO_2	0.01	0.03	0.01	0.02	0.01	0.02	0.00	0.03	0.02	0.02	0.01	0.02	0.00	0.00	0.00	0.00	0.00	0.00
Al_2O_3	0.64	0.64	0.54	0.30	0.21	0.59	0.74	0.59	0.38	0.76	0.27	0.32	0.74	0.25	0.39	0.58	0.37	0.51
Cr_2O_3	0.04	0.03	0.03	0.00	0.02	0.07	0.04	0.04	0.00	0.07	0.02	0.00	0.06	0.00	0.00	0.00	0.00	0.00
FeO	2.63	2.62	2.54	2.42	2.36	2.41	2.52	2.69	2.47	2.62	2.21	2.38	2.40	1.90	2.07	1.79	2.21	2.08
MnO	0.05	0.03	0.09	0.08	0.03	0.08	0.08	0.09	0.09	0.02	0.01	0.02	0.00	0.00	0.00	0.00	0.00	0.00
MgO	38.69	38.43	38.89	38.54	38.07	38.37	38.39	37.91	38.15	38.39	38.48	38.45	38.21	39.88	39.31	39.89	39.93	40.04
CaO	0.03	0.02	0.04	0.04	0.01	0.00	0.04	0.01	0.01	0.03	0.01	0.00	0.03	0.00	0.00	0.00	0.00	0.00
Na_2O	0.01	0.03	0.07	0.01	0.00	0.02	0.07	0.01	0.03	0.15	0.02	0.01	0.07	0.02	0.01	0.01	0.01	0.01
K_2O	0.00	0.01	0.02	0.01	0.00	0.00	0.01	0.01	0.00	0.02	0.00	0.02	0.03	0.00	0.00	0.00	0.00	0.00
P_2O_5	0.01	0.02	0.03	0.06	0.03	0.02	0.02	0.00	0.02	0.00	0.01	0.03	0.02	0.00	0.00	0.00	0.00	0.00
Total	85.61	85.21	85.70	85.22	83.63	84.75	84.23	84.34	84.22	85.61	85.81	85.54	85.32	87.10	86.80	87.08	87.49	87.53
Si	2.055	2.056	2.050	2.072	2.070	2.057	2.034	2.061	2.066	2.056	2.098	2.086	2.069	2.081	2.086	2.069	2.071	2.065
Ti	0.000	0.001	0.000	0.001	0.000	0.001	0.000	0.001	0.001	0.001	0.000	0.001	0.000	0.000	0.000	0.000	0.000	0.000
Al	0.035	0.035	0.030	0.017	0.012	0.033	0.042	0.034	0.021	0.042	0.015	0.018	0.041	0.013	0.021	0.031	0.020	0.028
Cr	0.001	0.001	0.001	0.000	0.001	0.003	0.001	0.002	0.000	0.003	0.001	0.000	0.002	0.000	0.000	0.000	0.000	0.000
Fe	0.104	0.104	0.100	0.096	0.095	0.096	0.101	0.108	0.099	0.103	0.087	0.094	0.095	0.073	0.080	0.069	0.085	0.080
Mn	0.002	0.001	0.004	0.003	0.001	0.003	0.003	0.004	0.004	0.001	0.000	0.001	0.000	0.000	0.000	0.000	0.000	0.000
Mg	2.724	2.716	2.735	2.721	2.739	2.726	2.750	2.710	2.728	2.703	2.689	2.700	2.692	2.745	2.716	2.746	2.742	2.747
Ca	0.001	0.001	0.002	0.002	0.001	0.000	0.002	0.000	0.000	0.002	0.000	0.000	0.001	0.000	0.000	0.000	0.000	0.000
Na	0.001	0.003	0.006	0.001	0.000	0.002	0.006	0.000	0.002	0.014	0.002	0.001	0.006	0.001	0.001	0.000	0.001	0.001
K	0.000	0.001	0.001	0.000	0.000	0.000	0.000	0.000	0.000	0.001	0.000	0.001	0.002	0.000	0.000	0.000	0.000	0.000
P	0.001	0.001	0.001	0.003	0.001	0.001	0.001	0.000	0.001	0.000	0.001	0.001	0.001	0.000	0.000	0.000	0.000	0.000
Total	4.925	4.920	4.931	4.916	4.919	4.922	4.941	4.920	4.922	4.926	4.894	4.902	4.910	4.913	4.904	4.916	4.919	4.921

	M2																
	#14	#15	#16	#17	#18	#19	#20	#21	#27	#28	#29	#30	#31	#32	#33	#34	#38
SiO_2	44.51	44.76	45.09	44.54	44.93	44.19	45.39	44.40	44.78	44.96	44.65	44.75	44.58	45.02	44.59	45.04	44.90
TiO_2	0.00	0.00	0.00	0.00	0.00	0.00	0.00	0.00	0.00	0.00	0.00	0.00	0.00	0.00	0.00	0.00	0.00
Al_2O_3	0.72	0.39	0.41	0.48	0.36	0.23	0.16	0.40	0.57	0.59	0.61	0.40	0.45	0.53	0.48	0.45	0.54
Cr_2O_3	0.00	0.00	0.00	0.00	0.00	0.00	0.00	0.00	0.00	0.00	0.00	0.00	0.00	0.00	0.00	0.00	0.00
FeO	1.95	2.02	1.84	2.11	1.85	1.77	1.75	1.82	1.86	1.75	2.13	1.81	1.82	1.75	2.00	2.05	2.32
MnO	0.00	0.00	0.00	0.00	0.00	0.00	0.00	0.00	0.00	0.00	0.00	0.00	0.00	0.00	0.00	0.00	0.00
MgO	39.64	40.07	40.48	39.46	39.99	39.73	40.26	39.68	39.76	40.07	39.57	40.04	39.99	40.42	39.80	39.91	39.71
CaO	0.00	0.00	0.00	0.00	0.00	0.00	0.00	0.00	0.00	0.00	0.00	0.00	0.00	0.00	0.00	0.00	0.00
Na_2O	0.02	0.01	0.00	0.02	0.01	0.00	0.01	0.00	0.04	0.00	0.02	0.02	0.00	0.01	0.00	0.02	0.03
K_2O	0.00	0.00	0.00	0.00	0.00	0.00	0.00	0.00	0.00	0.00	0.00	0.00	0.00	0.00	0.00	0.00	0.00
P_2O_5	0.00	0.00	0.00	0.00	0.00	0.00	0.00	0.00	0.00	0.00	0.00	0.00	0.00	0.00	0.00	0.00	0.00
Total	86.84	87.25	87.83	86.62	87.15	85.93	87.58	86.31	87.01	87.38	86.97	87.02	86.84	87.74	86.89	87.47	87.50

Table 2 (continued)

	M2																
	#14	#15	#16	#17	#18	#19	#20	#21	#27	#28	#29	#30	#31	#32	#33	#34	#38
Si	2.063	2.066	2.066	2.071	2.074	2.069	2.083	2.069	2.070	2.068	2.068	2.069	2.065	2.064	2.067	2.073	2.069
Ti	0.000	0.000	0.000	0.000	0.000	0.000	0.000	0.000	0.000	0.000	0.000	0.000	0.000	0.000	0.000	0.000	0.000
Al	0.039	0.021	0.022	0.026	0.020	0.012	0.009	0.022	0.031	0.032	0.033	0.022	0.024	0.028	0.026	0.024	0.029
Cr	0.000	0.000	0.000	0.000	0.000	0.000	0.000	0.000	0.000	0.000	0.000	0.000	0.000	0.000	0.000	0.000	0.000
Fe	0.075	0.078	0.070	0.082	0.071	0.069	0.067	0.071	0.072	0.067	0.082	0.070	0.070	0.067	0.077	0.079	0.089
Mn	0.000	0.000	0.000	0.000	0.000	0.000	0.000	0.000	0.000	0.000	0.000	0.000	0.000	0.000	0.000	0.000	0.000
Mg	2.739	2.757	2.765	2.736	2.751	2.774	2.754	2.757	2.740	2.748	2.732	2.759	2.762	2.762	2.750	2.738	2.728
Ca	0.000	0.000	0.000	0.000	0.000	0.000	0.000	0.000	0.000	0.000	0.000	0.000	0.000	0.000	0.000	0.000	0.000
Na	0.002	0.001	0.000	0.001	0.001	0.000	0.001	0.000	0.003	0.000	0.001	0.002	0.000	0.001	0.000	0.002	0.002
K	0.000	0.000	0.000	0.000	0.000	0.000	0.000	0.000	0.000	0.000	0.000	0.000	0.000	0.000	0.000	0.000	0.000
P	0.000	0.000	0.000	0.000	0.000	0.000	0.000	0.000	0.000	0.000	0.000	0.000	0.000	0.000	0.000	0.000	0.000
Total	4.918	4.924	4.923	4.917	4.917	4.925	4.914	4.920	4.916	4.916	4.916	4.921	4.922	4.923	4.921	4.916	4.918

They contain 42.16–45.39 wt% SiO_2, 36.51–41.5 wt% MgO, 0.0–0.76 wt% Al_2O_3, 1.23–7.33 wt% FeO, and 0.0–0.62 wt% Cr_2O_3.

The serpentine minerals form after retrograde hydrothermal alteration of ultramafic rocks or by prograde metamorphism of preexisting serpentinites (Deer et al. 1992). Lizardite is the most common retrograde reaction product, while antigorite is the most common prograde reaction product. Our petrographic studies, as well as x-ray diffraction data, revealed that the serpentine minerals of Jabal Shilman and Jabal Moqsim are mainly antigorite with subordinate chrysotile and lizardite. This indicates that parent minerals were first retrogressed to form chrysotile and lizardite and progressive metamorphism recrystallized these minerals into antigorite.

Chrome spinel

Representative analyses of chrome spinel and its alteration products are shown in Tables 3 and 4. Fresh chrome spinels are recorded only in the Jabal Shilman area, while altered chrome spinels are common in the Jabal Moqsim, because the analyzed samples from the latter are mylonitized and located along a shear zone. Fresh chrome spinels show high Cr_2O_3 contents (43.94–55.77 wt. %) and the Cr# (=Cr/Cr+Al) ranges from 0.62 to 0.79 with an average of 0.72. Altered chrome spinels are represented by ferritchromite and Cr-magnetite; the former is more common. The alteration of chromite to ferritchromite may have started during the late magmatic stage but is mainly due to later serpentinization and tectonism, perhaps associated with ophiolite emplacement (Khudeir et al. 1992).

The Cr–Al–Fe^{3+} diagram (Fig. 5a) is useful for distinguishing fresh and altered chrome spinels. On this diagram, altered chrome spinels plot along the Cr–Fe^{3+} join, reflecting loss of Al_2O_3 and Cr_2O_3 and increase in Fe_2O_3 due to alteration and metamorphism. Fresh chrome spinels lie along the Cr–Al join. On this diagram, spinels from Jabal Moqsim are altered whereas those from Jabal Shilman are relatively fresh. Consequently, we use Jabal Shilman spinels to infer petrogenesis of these ophiolitic ultramafics. Fresh Cr-spinels of Jabal Shilman are low in Al relative to Cr and are similar in this regard to ophiolitic podiform chromite associated with harzburgite (Fig. 5b).

Carbonates

Carbonates occur in the ultramafic rocks as sparse crystals or as cryptocrystalline veinlets. They are mostly magnesite and rarely dolomite (Table 5). Magnesite is an alteration product derived from magnesium-rich igneous and

Table 3 Microprobe analyses of chrome spinels in serpentinites of Jabal Shilman

	S2a						S6									
	#9	#11	#13	#14	#15	#16	#10	#11	#12	#31	#32	#34	#35	#36	#37	#38
SiO_2	0.00	0.00	0.00	0.00	0.00	0.00	0.00	0.00	0.00	0.00	0.00	0.00	0.00	0.00	0.00	0.00
TiO_2	0.10	0.12	0.10	0.13	0.10	0.10	0.23	0.25	0.23	0.30	0.29	0.28	0.30	0.32	0.25	0.31
Al_2O_3	17.64	17.97	16.85	17.30	17.72	17.83	10.28	9.75	9.81	11.09	10.86	11.34	10.80	10.93	10.52	11.17
Cr_2O_3	44.43	47.67	47.13	43.94	46.48	44.13	55.12	55.20	55.77	54.49	54.46	54.99	53.95	54.23	54.70	55.08
FeO	20.10	21.00	20.43	20.49	19.91	20.52	30.51	31.55	31.05	28.39	29.93	28.62	31.76	29.28	29.89	29.52
MnO	0.28	0.37	0.32	0.35	0.40	0.41	0.72	0.76	0.79	0.69	0.71	0.78	0.83	0.66	0.76	0.70
MgO	9.42	8.88	9.58	9.78	9.34	9.09	4.25	3.75	4.36	5.41	4.54	5.23	3.77	4.68	4.88	4.78
CaO	0.06	0.07	0.06	0.07	0.05	0.06	0.06	0.06	0.07	0.07	0.07	0.06	0.09	0.05	0.06	0.07
Na_2O	0.01	0.03	0.00	0.02	0.01	0.02	0.00	0.00	0.00	0.00	0.00	0.00	0.00	0.00	0.00	0.00
K_2O	0.02	0.01	0.04	0.02	0.02	0.01	0.00	0.00	0.00	0.00	0.00	0.00	0.00	0.00	0.00	0.00
P_2O_5	0.02	0.00	0.01	0.00	0.00	0.00	0.00	0.00	0.00	0.00	0.00	0.00	0.00	0.00	0.00	0.00
Total	92.01	96.08	94.46	92.06	93.99	92.13	101.15	101.33	102.08	100.44	100.85	101.30	101.51	100.15	101.06	101.63
Si	0.000	0.000	0.000	0.000	0.000	0.000	0.000	0.000	0.000	0.000	0.000	0.000	0.000	0.000	0.000	0.000
Ti	0.021	0.023	0.020	0.027	0.020	0.021	0.047	0.052	0.047	0.061	0.059	0.057	0.061	0.065	0.051	0.062
Al	5.726	5.639	5.362	5.604	5.652	5.790	3.289	3.133	3.116	3.532	3.468	3.583	3.449	3.509	3.351	3.534
Cr	9.676	10.034	10.060	9.549	9.946	9.613	11.835	11.902	11.885	11.638	11.671	11.659	11.556	11.684	11.686	11.688
Fe^{3+}	0.557	0.281	0.538	0.792	0.362	0.555	0.782	0.861	0.906	0.709	0.744	0.644	0.873	0.676	0.862	0.655
Fe^{2+}	4.072	4.394	4.076	3.917	4.144	4.172	6.146	6.334	6.093	5.704	6.041	5.773	6.323	5.997	5.892	5.971
Mn	0.065	0.084	0.073	0.082	0.091	0.096	0.165	0.176	0.181	0.158	0.162	0.176	0.190	0.153	0.174	0.158
Mg	3.867	3.525	3.855	4.006	3.770	3.734	1.720	1.523	1.753	2.179	1.835	2.091	1.522	1.900	1.967	1.911
Ca	0.017	0.020	0.016	0.021	0.015	0.018	0.017	0.018	0.020	0.020	0.020	0.017	0.026	0.015	0.017	0.021
Cr#	0.63	0.64	0.65	0.63	0.64	0.62	0.78	0.79	0.79	0.77	0.77	0.76	0.77	0.77	0.78	0.77
Mg#	0.49	0.45	0.49	0.51	0.48	0.47	0.22	0.19	0.22	0.28	0.23	0.27	0.19	0.24	0.25	0.24
Fe#	0.51	0.55	0.51	0.49	0.52	0.53	0.78	0.81	0.78	0.72	0.77	0.73	0.81	0.76	0.75	0.76

Table 4 Microprobe analyses of altered chrome spinels in serpentinites of Jabal Moqsim

	M1									M2					
	#14	#15	#11	#12	#13	#16	#17	#18	#19	#7	#9	#12	#13	#24	#26
SiO_2	0.00	1.29	0.20	0.39	0.00	0.07	0.00	0.15	0.00	0.02	0.03	0.03	0.03	0.11	0.04
TiO_2	0.18	0.19	0.20	0.19	0.18	0.18	0.19	0.20	0.17	0.05	0.00	0.02	0.04	0.03	0.04
Al_2O_3	0.16	0.23	0.11	0.12	0.10	0.12	0.13	0.12	0.12	0.05	0.10	0.08	0.06	0.08	0.08
Cr_2O_3	33.56	34.26	12.62	6.18	3.14	12.47	4.41	14.37	9.22	32.48	36.35	34.73	33.83	33.84	31.76
FeO	61.32	57.70	82.37	90.05	94.39	82.82	91.56	80.81	87.46	61.31	57.39	59.44	59.41	59.69	62.31
MnO	1.82	1.96	0.78	0.36	0.25	0.71	0.33	0.86	0.54	1.70	1.83	1.78	1.78	1.77	1.68
MgO	0.98	2.22	0.32	0.35	0.00	0.19	0.00	0.32	0.04	1.39	1.77	1.40	1.45	1.55	1.23
CaO	0.09	0.09	0.10	0.09	0.12	0.09	0.12	0.11	0.08	0.00	0.00	0.00	0.00	0.00	0.00
Na_2O	0.04	0.07	0.04	0.05	0.00	0.00	0.03	0.03	0.01	0.04	0.01	0.03	0.04	0.04	0.02
K_2O	0.05	0.07	0.07	0.09	0.08	0.07	0.09	0.08	0.06	0.00	0.00	0.00	0.00	0.00	0.00
P_2O_5	0.11	0.06	0.15	0.15	0.13	0.13	0.16	0.15	0.10	0.04	0.00	0.00	0.00	0.02	0.00
Total	98.93	98.80	97.29	98.29	98.63	97.09	97.21	97.64	98.15	97.19	97.61	97.69	96.83	97.23	97.30
Si	0.000	0.374	0.058	0.114	0.000	0.022	0.000	0.043	0.000	0.007	0.010	0.008	0.010	0.034	0.012
Ti	0.040	0.042	0.045	0.041	0.039	0.040	0.041	0.044	0.038	0.011	0.000	0.003	0.008	0.006	0.008
Al	0.054	0.079	0.039	0.040	0.034	0.040	0.044	0.043	0.040	0.019	0.035	0.028	0.020	0.027	0.029
Cr	7.789	7.867	2.952	1.433	0.726	2.942	1.036	3.378	2.152	7.648	8.507	8.145	8.002	7.957	7.473
Fe^{3+}	8.077	7.223	12.804	14.216	15.162	12.895	14.838	12.404	13.732	8.298	7.438	7.804	7.941	7.938	8.459
Fe^{2+}	6.975	6.790	7.579	7.885	7.941	7.771	7.921	7.693	7.859	6.971	6.769	6.943	6.922	6.908	7.049
Mn	0.452	0.481	0.195	0.090	0.061	0.180	0.082	0.217	0.134	0.430	0.459	0.448	0.452	0.447	0.424
Mg	0.430	0.961	0.139	0.151	0.000	0.083	0.000	0.143	0.019	0.617	0.782	0.621	0.645	0.685	0.546
Ca	0.027	0.028	0.031	0.029	0.036	0.028	0.038	0.034	0.026	0.000	0.000	0.000	0.000	0.000	0.001
Cr#	0.99	0.99	0.99	0.97	0.96	0.99	0.96	0.99	0.98	1.00	1.00	1.00	1.00	1.00	1.00
Mg#	0.06	0.12	0.02	0.02	0.00	0.01	0.00	0.02	0.00	0.08	0.10	0.08	0.09	0.09	0.07
Fe#	0.94	0.88	0.98	0.98	1.00	0.99	1.00	0.98	1.00	0.92	0.90	0.92	0.91	0.91	0.93

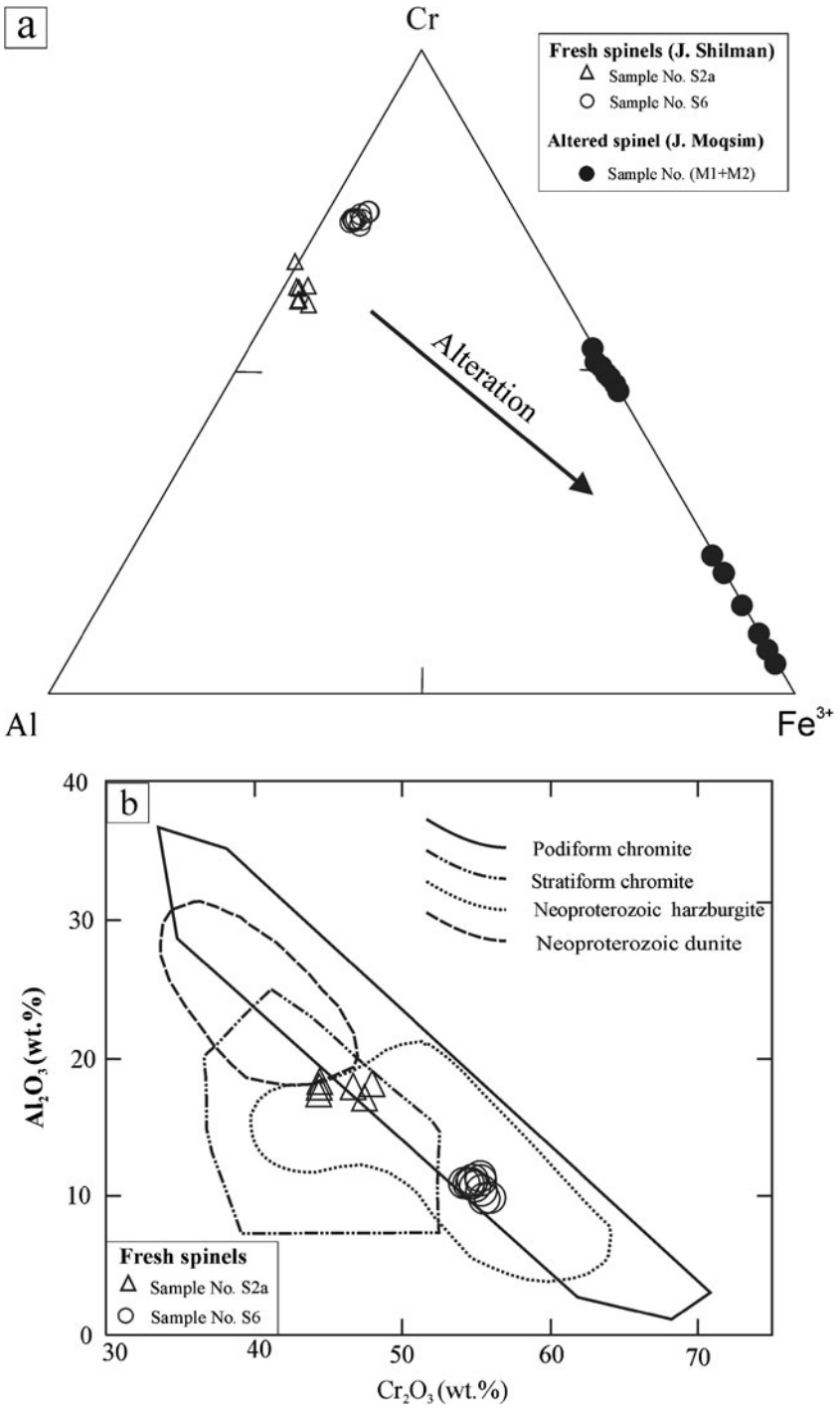

Fig. 5 **a** Cr–Al–Fe^{3+} plot of Jabal Shilman and Jabal Moqsim chrome spinels and their alteration products, and **b** Al_2O_3 versus Cr_2O_3 for the analyzed accessory fresh chrome spinels (Bonavia et al. 1993)

metamorphic rocks (Deer et al. 1992). The substitution of Mn and Fe for Mg is limited. The sparse magnesite crystals may have been formed during serpentinization or somewhat later during low- to medium-grade metamorphism in the presence of CO_2. The monomineralic and cryptocrystalline character of the magnesite veinlets indicate precipitation from CO_2-rich solutions at near surface conditions (Abu-Jaber and Kimberley 1992). So, the magnesite veinlets might be ascribed to local shearing accompanied by infiltration of solutions rich in CO_2.

Geochemical characteristics

Representative chemical analyses of Jabal Shilman and Jabal Moqsim peridotites are given in Table 6. All the serpentinites have high LOI values (11.43 to 18.46 wt. %) which indicates the hydrous nature of these rocks. They show high MgO (35.3 to 43.2 wt. %) and moderate Fe_2O_3 (6.17 to 8.29 wt. %). CaO content is usually low (0.02 to 0.66 wt %), but is higher in few samples (1.14 to 2.64 wt. %) due to the presence of secondary carbonates, particularly in the more altered ultramafics of

Table 5 Microprobe analyses of altered carbonates in serpentinites of Jabal Shilman and Jabal Moqsim

	Magnesite									Dolomite				
	Jabal Shilman		Jabal Moqsim							Jabal Moqsim				
	S2a		M1				M2			M1			S6	
	#19	#20	#24	#25	#26	#27	#35	#36	#37	#8	#22	#23	#15	#25
SiO_2	2.15	0.10	0.00	0.00	0.18	0.00	0.00	0.00	0.00	0.00	0.00	0.00	0.00	0.00
TiO_2	0.02	0.03	0.00	0.00	0.00	0.00	0.00	0.00	0.00	0.02	0.01	0.03	0.04	0.03
Al_2O_3	0.00	0.00	0.00	0.00	0.00	0.00	0.00	0.00	0.00	0.00	0.01	0.02	0.00	0.00
Cr_2O_3	0.07	0.00	0.00	0.00	0.00	0.00	0.00	0.00	0.00	0.03	0.03	0.00	0.06	0.08
FeO	0.49	0.38	1.53	1.52	1.82	1.50	1.02	0.93	1.08	0.58	0.55	0.36	2.50	2.03
MnO	1.25	1.23	0.49	0.49	0.53	0.55	0.13	0.16	0.06	0.22	0.16	0.24	0.89	0.42
MgO	46.51	47.35	47.55	46.39	46.61	47.64	48.30	48.00	47.99	21.11	21.22	21.22	21.22	21.34
CaO	0.19	0.13	0.23	0.12	0.09	0.11	0.07	0.02	0.02	29.73	28.28	29.28	34.32	33.36
Na_2O	0.01	0.00	0.00	0.01	0.00	0.00	0.00	0.01	0.00	0.00	0.02	0.01	0.00	0.02
K_2O	0.00	0.00	0.00	0.00	0.00	0.00	0.00	0.00	0.00	0.00	0.01	0.01	0.01	0.04
P_2O_5	0.00	0.00	0.05	0.05	0.00	0.01	0.00	0.00	0.00	0.08	0.09	0.01	0.06	0.07
F	0.00	0.00	0.01	0.00	0.00	0.01	0.00	0.00	0.00	0.00	0.07	0.05	0.01	0.00
Cl	0.02	0.01	0.00	0.00	0.00	0.00	0.00	0.00	0.00	0.00	0.00	0.00	0.01	0.07
SO_2	0.00	0.01	0.02	0.03	0.00	0.02	0.00	0.00	0.00	0.02	0.01	0.06	0.07	0.03
Total	50.71	49.23	49.88	48.61	49.24	49.85	49.53	49.12	49.14	51.79	50.47	51.27	59.18	57.49

Table 6 Chemical analyses of serpentinites of Jabal Shilman and Jabal Moqsim

Rock type	Serpentinite											
Location	Jabal Shilman					Jabal Moqsim						
Sample No	S2a	S4	S6	SH-6[a]	SH-7[a]	M5	M9	M13	M1	M2	M8	M12
SiO_2	36.6	36.25	40.28	36.55	37.16	43.07	42.59	43.22	38.64	38.37	37.85	35.26
TiO_2	0.002	0.001	0.007	< 0.01	< 0.01	0.01	0.00	0.01	0.001	0.002	0.001	0.004
Al_2O_3	0.33	0.33	1.29	0.22	0.39	0.33	0.38	0.77	0.51	0.55	0.17	0.27
$Fe_2O_{3(T)}$	7.34	7.26	8.29	6.47	7.27	6.17	6.29	6.31	7.21	7.64	6.21	6.73
MnO	0.084	0.087	0.079	0.08	0.07	0.08	0.10	0.10	0.09	0.083	0.08	0.089
MgO	37.94	38.16	35.11	37.41	38.34	38.31	37.87	34.69	38.92	37.16	37.41	37.42
CaO	0.35	0.35	0.51	0.34	0.25	0.17	0.02	2.64	0.81	1.14	0.66	0.08
Na_2O	0.02	< 0.01	0.01	0.01	0.02	< 0.01	< 0.01	0.01	0.01	< 0.01	< 0.01	< 0.01
K_2O	< 0.01	< 0.01	< 0.01	0.02	0.01	< 0.01	< 0.01	< 0.01	< 0.01	< 0.01	< 0.01	< 0.01
P_2O_5	< 0.01	< 0.01	< 0.01	0.01	0.01	0.04	0.04	0.10	< 0.01	< 0.01	< 0.01	< 0.01
LOI	15.47	15.82	12.51	17.40	15.30	11.56	11.43	11.46	14.6	13.94	16.37	18.46
Total	98.136	98.258	98.086	98.51	98.82	99.74	98.72	99.31	100.79	98.885	98.751	98.313
Mg#	91.10	91.24	89.35	91.97	91.27	92.48	92.27	91.59	91.45	90.60	92.27	91.68
Ba	3	12	10	48	49	9	115	194	6	14	8	2
Sr	4	4	12	176	180	13	< 2	18	8	18	6	< 2
Y	< 1	< 1	< 1	2.5	3.1	< 1	< 1	2	< 1	< 1	< 1	< 1
Sc	6	6	4	34	29	4	6	5	6	7	4	5
Zr	5	3	3	7	6	15	15	12	16	3	3	2
Be	< 1	< 1	< 1	–	–	< 1	< 1	< 1	< 1	< 1	< 1	< 1
V	22	21	28	576	583	15	19	21	28	30	16	19

[a] Analyses adopted from Azer (2012)

Jabal Moqsim. These compositions, except for high water contents, are similar to those of fresh peridotites and indicate limited mobility of Mg and Fe. Ca- metasomatism is a common concern in Egyptian serpentinites because of pervasive carbonate alteration (Stern and Gwinn 1990), but the low and restricted range of CaO and its covariance with Al_2O_3 contents in the studied serpentinites suggests that this was limited in the analyzed samples.

The serpentinites show high Mg# (100 molar Mg/Mg+Fe), from 89.4 to 91.2 (mean =90.6) in Jabal Shilman, slightly higher in Jabal Moqsim (from 90.6 to 92.5; mean =91.8). These Mg-numbers for the studied serpentinized peridotites are at the upper range of modern oceanic peridotite Mg#s (Bonatti and Michael 1989). On the Al_2O_3-MgO-CaO diagram (Fig. 6a), the Ca-depleted nature of the serpentinites is clear, and they plot within the field of metamorphic peridotites associated with ophiolites (Coleman 1977). The MgO/ (MgO+FeO) ratios of the analyzed serpentinites range from 0.81 to 0.86 with an average of 0.84. This average is similar to that of the metamorphic lherzolites (0.84) and metamorphic harzburgites (0.85) given by Coleman (1977). The computed normative proportions of olivine, orthopyroxene and clinopyroxene of the analyzed serpentinites are plotted on Ol-Opx-Cpx diagram (Fig. 6b). The studied serpentinites fall within the harzburgite field, except sample no. M13 falls in the lherzolite field.

Petrographic and geochemical data indicate that, unless carbonated, addition or subtraction of elements other than water and perhaps silica was limited for the studied serpentinized peridotites. Therefore, it is useful to compare the studied ultramafics with peridotites from modern tectonic settings. The serpentinites of Jabal Shilman and Jabal Moqsim have very low abundances of Al_2O_3 (0.17-1.1.29 wt.

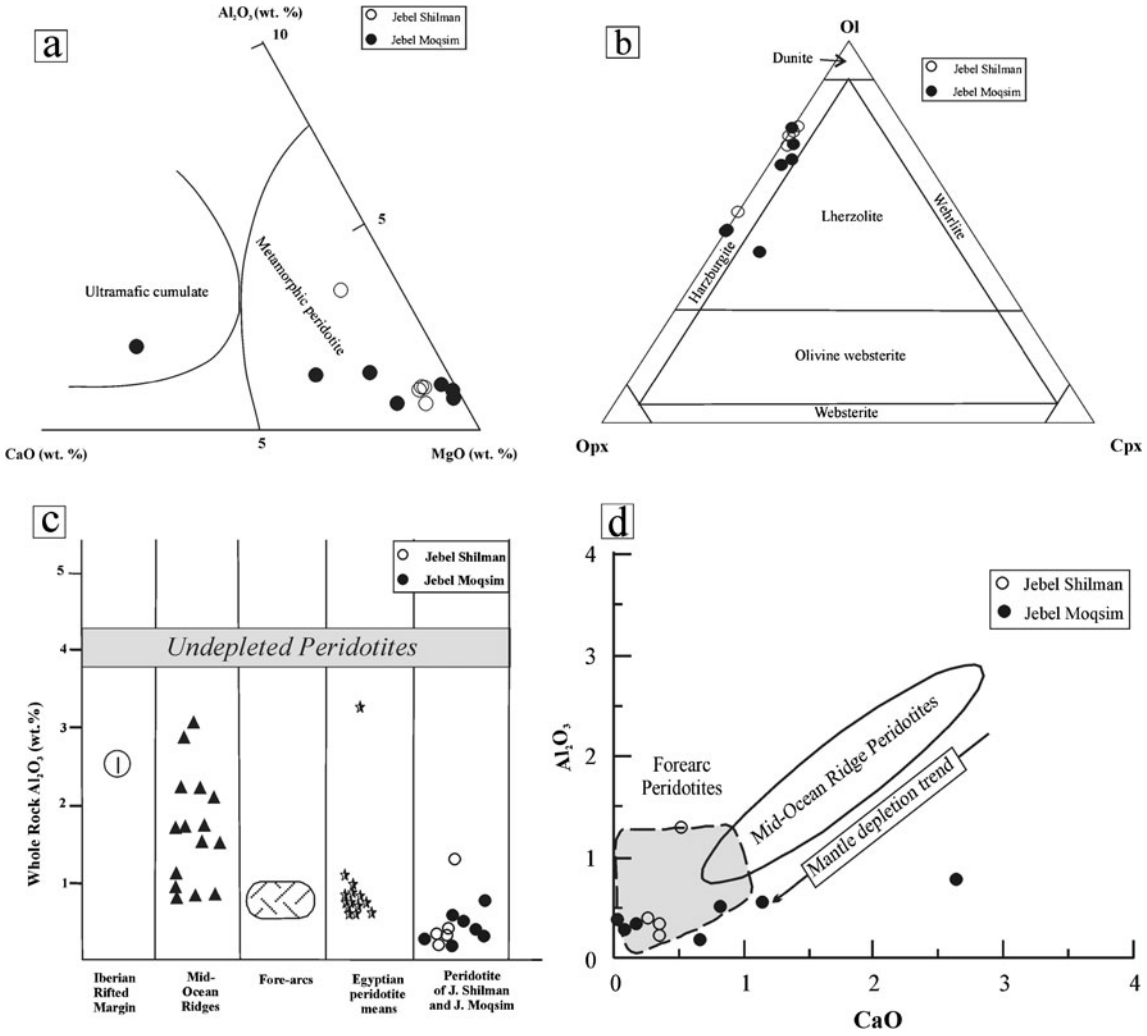

Fig. 6 **a** Al_2O_3–MgO–CaO diagram for the studied serpentinites (Coleman 1977), **b** Ol–Cpx–Opx normative composition of the studied serpentinites (Coleman 1977), **c**Whole-rock Al_2O_3 content in Jabal Shilman and Jabal Moqsim serpentinites and in other Egyptian Neoproterozoic serpentinized peridotites compared with peridotites from other tectonic settings (modified after Bonatti and Michael 1989); the means of the different localities in the Eastern Desert of Egypt are adopted from Azer and Stern (2007), and **d** Al_2O_3 vs. CaO diagram (after Ishii et al. 1992) for comparing Jabal Shilman and Jabal Moqsim serpentinites with peridotites from other tectonic settings

%), similar to peridotites from modern fore-arcs and Neoproterozoic serpentinized peridotites from the Central Eastern Desert (Fig. 6c). Moreover, on the Al_2O_3 vs. CaO diagram (Fig. 6d) most of the analyzed samples are depleted in Al_2O_3 and CaO, similar to fore-arc peridotites.

Discussion: tectonic setting and petrogenesis

ANS ophiolitic rocks have long been the subject of research because they represent important elements for reconstructing its geodynamic evolution. They are generally interpreted to have been generated in suprasubduction zone tectonic settings (e.g. Nassief et al. 1984; Pallister et al. 1988; Stern et al. 2004); similar interpretations hold for Egyptian ophiolitic rocks (e.g. El Sayed et al. 1999; Ahmed et al. 2001; Farahat et al. 2004; Azer and Stern 2007; Khalil and Azer 2007; Abd El-Rahman et al. 2009a, b). By contrast, MOR tectonic setting has been inferred for the origin of Gerf and Ghadir ophiolites in Egypt (Zimmer et al. 1995; Basta et al. 2011). Studies of the ANS ophiolitic lavas often infer a back-arc basin geodynamic setting, but studies of the ANS ophiolitic peridotites recognize similarities to modern fore-arc peridotites. Seafloor spreading during subduction initiation is thought to form forearc ophiolites (Pearce 2003; Stern 2004). The controversy about the tectonic setting where ANS ophiolites formed is important because fore-arc ophiolites mark episodes when new subduction zones form (Stern 2004), episodes that are associated with major plate reorganizations. In contrast, back-arc basins can form at any time in the evolution of a convergent plate margin.

Assessments of tectonic setting for ANS ophiolites in general and the Eastern Desert ophiolites specifically have focused mostly on the trace element contents of lavas but increasingly consider evidence from the abundant serpentinites. Interpreting tectonic setting of the Neoproterozoic ophiolitic rocks on the basis of major- and trace-element compositions of metavolcanic rocks encounters difficulties due to effects of fractional crystallization and alteration. Even when these problems are minimized, it can be very difficult to distinguish fore-arc and back-arc lavas on a basis of chemical compositions (Azer and Stern 2007). Most researchers recognize that ANS ophiolitic lavas show transitional geochemical character between those of island arcs and MORBs and on this basis, a back-arc basin environment of formation is often inferred (e.g. El Sayed et al. 1999; Farahat et al. 2004; Abd El-Rahman et al. 2009b; Farahat 2010). Formation in a fore-arc setting during subduction initiation is increasingly considered for Egyptian ophiolites (Azer and Stern 2007; Khalil and Azer 2007; Abd El-Rahman et al. 2009a), partly because the hypothesis of fore-arc spreading during subduction initiation is relatively new (Shervais et al. 2004; Stern 2004).

Spinel and whole rock compositions of Allaqi peridotites must be considered together for constraining petrogenesis and thus tectonic setting. Chromite is the only primary mineral retained in the studied serpentinized peridotite, but even spinels can be affected during pervasive serpentinization, as shown by Jabal Moqsim peridotite spinels, which are ferritchromite recognizable by very low MgO contents

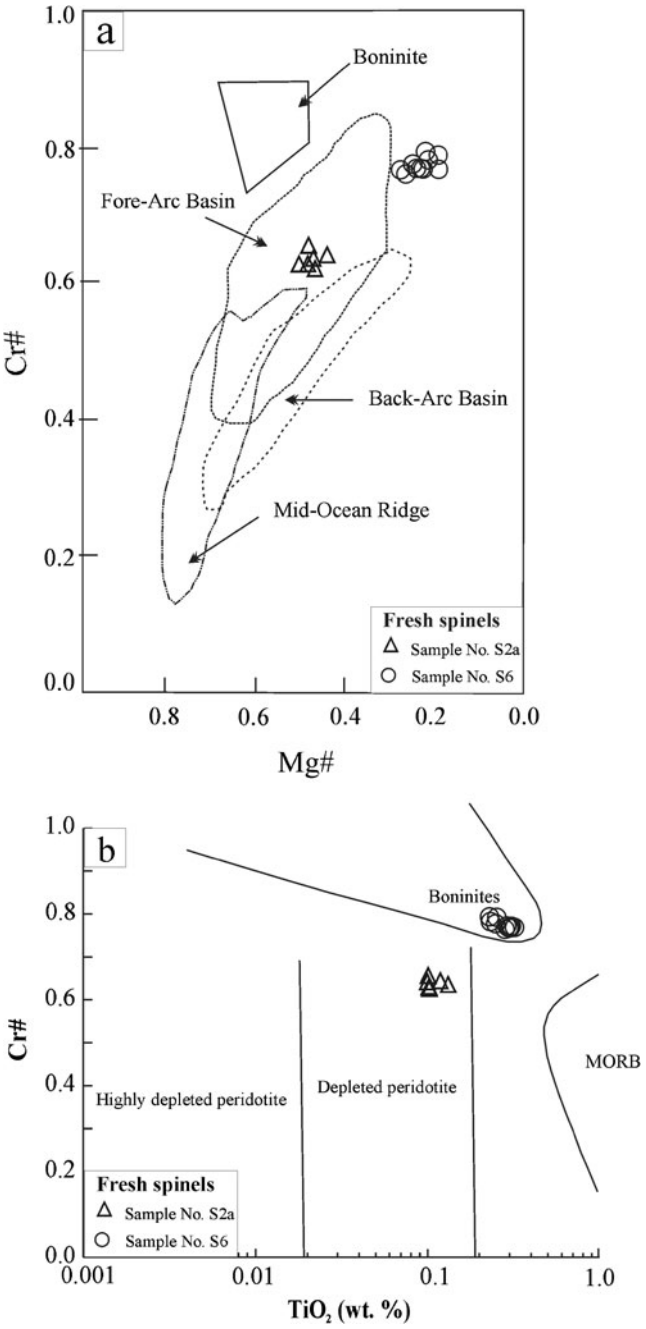

Fig. 7 **a** Cr# vs. Mg# diagram for fresh chrome spinels (after Stern et al. 2004); the field boundaries are from Dick and Bullen (1984), Bloomer et al. (1995) and Ohara et al. (2002), and **b** Cr# vs. TiO_2 diagram for the analyzed accessory fresh chrome spinels (fields after Dick and Bullen 1984; Arai 1992; Jan and Windley 1990)

and very high FeO contents. Our study shows that such alteration can be identified so that even completely serpentinized ultramafic rocks containing no relicts of primary silicate minerals, the chemical composition of the relict spinels can be used. This approach has enjoyed wide success for other ophiolites (Irvine 1965; Dick and Bullen 1984; Jan and Windley 1990; Arai 1992; Sack and Ghiorso 1991; Barnes and Roeder 2001; Sobolev and Logvinova 2005; Arif and Jan 2006). Global studies indicate that spinels from MOR peridotites generally have Cr# < 50, while spinels in fore-arc harzburgites generally have higher Cr# (up to 80) and spinels from boninites typically have Cr# of 70–90 (Barnes and Roeder 2001; Ohara et al. 2002; Morishita et al. 2011). Chemical analyses of the fresh chrome spinels in the Jabal Shilman serpentinized peridotites are plotted on Cr# versus Mg# diagram (Fig. 7a), which shows that Shilman spinels have high Cr# (av. 0.72), similar to that of modern fore-arc peridotites. The harzburgitic composition and low CaO contents in the studied serpentinized peridotites indicates that the protoliths were poor in clinopyroxene and suggest affinities similar to the most depleted oceanic peridotites, which today are found in forearcs (Bonatti and Michael 1989). High Cr# for relict spinels and low abundances of Al_2O_3 and CaO in the Allaqi peridotites are both consistent with a harzburgite parent (Dick and Bullen 1984) and are very similar to the composition of fore-arc peridotites (Fig. 6c, d; Ishii et al. 1992).

The depleted nature of the studied serpentinites is confirmed by using the Cr# vs. TiO_2 diagram for the fresh chrome spinels (Fig. 7b). The highly depleted peridotites with high Cr# (>0.7) of spinels can be produced in the mantle wedge beneath arcs or in plume-related within-plate mantle (Pearce et al. 1984; Arai 1994; Ishiwatari et al. 2003). The TiO_2 content of spinel reflects the tectonic site of magma generation; TiO_2 is low in arc magmas, intermediate in MORBs and high in intraplate magmas (Arai 1992). High Cr# and low TiO_2 as well as their depleted nature for the analyzed chrome spinels suggest an origin from a mantle wedge or a sub-arc mantle. The mineral and whole-rock chemical data reported here indicate that the serpentinized peridotites of Jabal Shilman and Jabal Moqsim formed as highly-depleted mantle residues, similar to those in peridotites from fore-arc regions of subduction zone. Therefore, the studied serpentinized peridotites represent a fragment of oceanic lithosphere that formed in a fore-arc environment (Fig. 8); that is, they belong to an ophiolitic mantle sequence formed in a supra-subduction zone.

Conclusion

In this study, we used the results of the first study of the geology, petrology, mineral chemistry and geochemistry of ophiolitic ultramafic rocks along Wadi Allaqi to assess the geodynamic evolution of this part of the ANS. Neoproterozoic ophiolitic peridotites of the studied areas occur within a regionally metamorphosed metasediment-metavolcanic rocks and define the southernmost ophiolitic ultramafic rocks in the Eastern Desert of Egypt. They were thrust over the associated island arc calc-alkaline metavolcanics and replaced by talc carbonates along shear zones probably due to CO_2-metasomatism.

The serpentinites show a prevalence of mesh and bastite textures, suggesting derivation from harzburgite and dunite. The predominance of antigorite over other serpentine minerals indicates that the present serpentinites were first retrogressed to form chrysotile and lizardite. Then, progressive metamorphism recrystallized these minerals into antigorite,

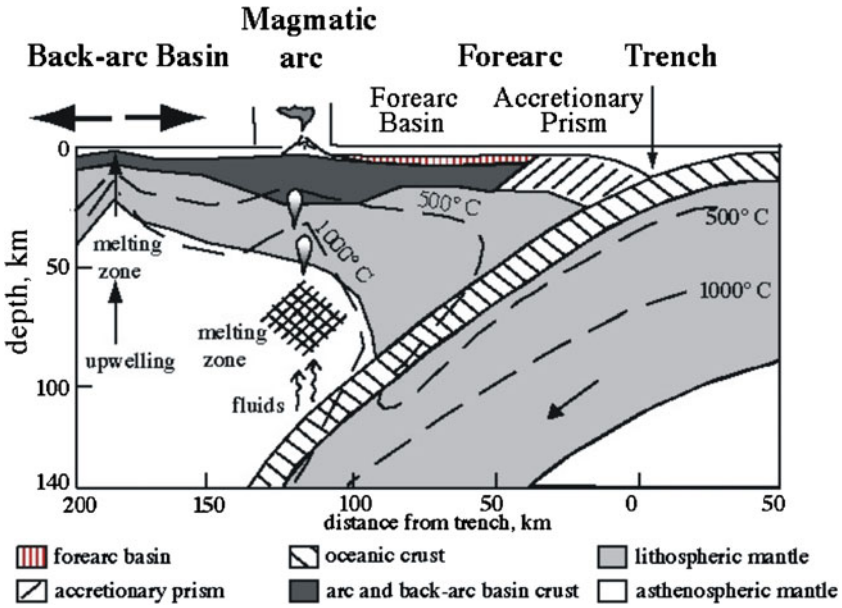

Fig. 8 Cartoon showing the tectonic setting of Jabal Shilman and Jabal Moqsim serpentinized peridotites in the fore-arc environment (adopted from Azer and Stern 2007)

probably during obduction. The presence of chrysotile as cross-fiber veinlets cutting across the other serpentine minerals indicates a late genesis as a result of the activity of meteoric waters.

The serpentinized peridotites of Jabal Shilman and Jabal Moqsim have high Mg# (89.35–92.48) and are depleted in Al_2O_3 and CaO similar to that of modern oceanic peridotites. They show compositions consistent with formation during the initiation of an intra-oceanic subduction. The primary chrome spinels in serpentinites have high Cr# (av. 0.72) similar to spinels in modern fore-arc peridotites. High Cr# in the analyzed chrome spinels indicates that they were generated by high degree of partial melting of depleted, harzburgitic to dunitic mantle peridotite, in an oceanic marginal basin environment. Therefore, the studied serpentinites represent a fragment of oceanic lithosphere that formed in a fore-arc environment which belongs to an ophiolitic mantle sequence formed above a subduction zone.

There is much more work that needs to be carried out on the ophiolitic rocks of the Allaqi-Heiani suture, but this study shows some of the insights that can be gained by such studies.

Acknowledgments We highly appreciate thoughtful reviews by Kurt Stüwe (Associate Editor) and Shoji Arai (Kanazawa, Japan), which caused us to carry out a serious revision of the manuscript and improve it dramatically. This research was supported by NSF grant 0804749 (US-Egyptian Scientific Co-operation) to RJS and NSF EAR-0116660 for Electron Microprobe at UTEP.

References

Abd El-Naby HH, Frisch W (2002) Origin of the Wadi Haimur-Abu Swayel gneiss belt, south Eastern Desert, Egypt: Petrological and geochronological constraints. Precamb Res 113:307–322

Abd El-Rahman Y, Polat A, Dilek Y, Fryer BJ, El-Sharkawy M, Sakran S (2009a) Geohemistry and tectonic evolution of the Neoproterozoic incipient arc-fore-arc crust in the Fawakhir area, Central Eastern Desert of Egypt. Precamb Res 175:116–134

Abd El-Rahman Y, Polat A, Dilek Y, Fryer B, El-Sharkawy M, Sakran S (2009b) Geochemistry and tectonic evolution of the Neoproterozoic Wadi Ghadir ophiolite, Eastern Desert, Egypt. Lithos 113:158–178

Abdelsalam MG, Abdeen MM, Dowaidar HM, Stern RJ, Abdelghaffar AA (2003) Structural evolution of the Neoproterozoic Western Allaqi-Heiani suture, southeastern Egypt. Precamb Res 124:87–104

Abu El Ela FF, Farahat ES (2010) Neoproterozoic podiform chromites in serpentinites of the Abu Meriewa-Hagar Dungash district, Eastern Desert, Egypt: Geotectonic implications and metamorphism. Island Arc 19:151–164

Abu-Jaber NS, Kimberley MM (1992) Origin of ultramafic-hosted vein magnesite deposits. Ore Geol Rev 7:155–191

Ahmed AH, Arai S, Attia AK (2001) Petrological characteristics of podiform chromitites and associated peridotites of the Pan African ophiolite complexes of Egypt. Mineral Deposit 36:72–84

Ahmed AH, Hanghøj K, Kelemen PB, Hart SR, Arai S (2006) Osmium isotope systematics of the Proterozoic and Phanerozoic ophiolitic chromitites: In situ ion probe analysis of primary Os-rich PGM. Earth Planet Sci Lett 245:777–791

Ali KA, Azer MK, Gahlan HA, Wilde SA, Samuel MD, Stern RJ (2010) Age of formation and emplacement of Neoproterozoic ophiolites and related rocks along the Allaqi Suture, south Eastern Desert, Egypt. Gond Res 18:583–595

Andresen A, Abu El-Rus MA, Myhre PI, Boghdady GY, Corfu F (2009) U-Pb TIMS age constraints on he evolution of the Neoproterozoic Meatiq Gneiss Dome, Eastern Desert of Egypt. Inter J Earth Sci 98:481–497

Arai S (1992) Chemistry of chromian spinel in volcanic rocks as a potential guide to magma chemistry. Mineral Mag 56:173–184

Arai S (1994) Compositional variation of olivine-chromian spinel in Mg-rich magmas as a guide to their residual spinel peridotites. J Volcan Geoth Res 59:279–294

Arif M, Jan MQ (2006) Petrotectonic significance of the chemistry of chromite in the ultramafic-mafic complexes of Pakistan. J Asian Earth Sci 27:628–646

Azer MK (2008) Origin of Neoproterozoic Ophiolitic Serpentinites and Their Economic Potentialities, Eastern Desert, Egypt. 33th International Geological Congress, Oslo-Norway

Azer MK (2012) Evolution and economic significance of listwaenites associated with Neoproterozoic ophiolites in south Eastern Desert, Egypt. Geologica Acta (in press)

Azer MK, El-Gharbawy RI (2011) Contribution to the Neoproterozoic layered mafic-ultramafic intrusion of Gabal Imleih, south Sinai, Egypt: Implication of post-collisional magmatism in the north Arabian-Nubian Shield. J Afr Earth Sci 60:253–272

Azer MK, Khalil AES (2005) Petrological and mineralogical studies of Pan-African serpentinites at Bir Al-Edeid area. Cenatral Eastern Desert, Egypt. J Afr Earth Sci 43:525–536

Azer MK, Stern RJ (2007) Neoproterozoic (835–720 Ma) serpentinites in the Eastern Desert, Egypt: fragments of fore-arc mantle. J Geol 115:457–472

Barnes SJ, Roeder PL (2001) The range of spinel composition in terrestrial mafic ultramafic rocks. J Petrol 42:2279–2302

Basta FF, Maurice AE, Bakhit BR, Ali KA, Manton WI (2011) Neoproterozoic contaminated MORB of Wadi Ghadir ophiolite, NE Africa: geochemical and Nd and Sr isotopic constraints. J Afr Earth Sci 59:227–242

Berhe SM (1990) Ophiolites in Northeast and East Africa: implications for Proterozoic crustal growth. J Geol Soc London 147:41–57

Bloomer SH, Taylor B, MacLeod CJ, Stern RJ, Fryer P, Hawkins JW, Johnson L (1995) Early arc volcanism and ophiolite problem: a perspective from drilling in the Western Pacific. In: Taylor B, Natland J (eds) Active margins and marginal basins of the Western Pacific, Geophysical Monograph, Vol. 88. American Geophysical Union, Washington, DC, pp 1–30

Bonatti E, Michael PJ (1989) Mantle peridotites from continental rifts to oceanic basins to subduction zones. Earth Planet Sci Lett 91:297–311

Bonavia FF, Diella V, Ferrario A (1993) Precambrian podiform chromitites from Kenticha Hill, southern Ethiopia. Econ Geol 88:198–202

Coleman RG (1977) Ophiolites. Springer-Verlag, Berlin, 229

De Wall H, Greiling RO, Sadek MF (2001) Post-collisional shortening in the Late Pan-African Hamisana high strain zone SE Egypt: field and magnetic fabric evidence. Precamb Res 107:179–194

Deer WA, Howie RA, Zussman J (1992) An introduction to the rock forming minerals, 2nd edn. Longman scientific and technical, London, 696

Dick HB, Bullen T (1984) Chromian spinel as a petrogenetic indicator in abyssal and Alpine-type peridotites and spatially associated lavas. Contrib Mineral Petrol 86:54–76

Dilek Y, Ahmed Z (2003) Proterozoic ophiolites of the Arabian Shield and their significance in Precambrian tectonics. In: Dilek Y,

Robinson PT (eds) Ophiolites in Earth History. Geol Soc London Spec Publ 218:685–700

Dixon TH (1979) Evolution of continental crust in the Late Precambrian Egyptian Shield. Thesis, University of California, San Diego

Dixon TH (1981a) Gebel Dahanib, Egypt: a late Precambrian layered sill of komatiitic composition. Contrib Mineral Petrol 76:42–52

Dixon TH (1981b) Age and chemical characteristics of some pre-Pan-african rocks in the Egyptian Shield. Precamb Res 14:119–133

El Bahariya GA, Arai S (2003) Petrology and origin of Pan-African serpentinites with particular reference to chromian spinel compositions, Eastern Desert, Egypt: implication for supra-subduction zone ophiolite. 3rd Inter Conf Geol Afr 371–388

El Gaby S, List FK, Tehrani R (1988) Geology, evolution and metallogenesis of the Pan-African Belt in Egypt. In: El Gaby, S, Greiling RO (eds) The Pan-African Belt of northeast Africa and adjacent areas. Braunschweig Viewig 17–68

El Sayed MM, Furnes H, Mohamed FH (1999) Geochemical constraints on the tectonomagmatic evolution of the late Precambrian Fawakhir ophiolite, Central eastern Desert, Egypt. J Afr Earth Sci 29:515–533

El Sharkawy MA, El Bayoumi RM (1979) The ophiolites of Wadi Ghadir area, Eastern Desert, Egypt. Ann Geol Surv Egypt 9:125–135

El-Kazzaz YA, Taylor WEG (2001) Tectonic evolution of the Allaqi Shear zone and implications for Pan-African terrane amalgamation in the southern Eastern Desert, Egypt. J Afr Earth Sci 33:177–197

El-Nisr S (1997) Late Precambrian volcanism at Wadi Allaqi, south Eastern Desert, Egypt: Evidence for transitional continental arc/margin environment. J Afr Earth Sci 24:301–313

Farahat ES (2008) Chrome-spinels in serpentinites and talc carbonates of the El Ideid-El-Sodmein District, central Eastern Desert, Egypt: their metamorphism and petrogenetic implications. Chem Erde 68:193–205

Farahat ES (2010) Neoproterozoic arc-back-arc system in the central Eastern Desert of Egypt: evidence from supra-subduction zone ophiolites. Lithos 120:293–308

Farahat ES, Helmy HM (2006) Abu hamamid neoproterozoic alaskan-type complex, south Eastern Desert, Egypt. J Afr Earth Sci 45:187–197

Farahat ES, El Mahalawi MM, Hoinkes G (2004) Continental back-arc basin origin of some ophiolites from the Eastern Desert of Egypt. Mineral Petrol 82:81–104

Gahlan H, Arai S (2009) Carbonate-orthopyroxenite lenses from the Neoproterozoic Gerf ophiolite, South Eastern Desert, Egypt: The first record in the Arabian Nubian Shield ophiolites. J Afr Earth Sci 53:70–82

Greiling RO, Kröner A, El Ramly MF, Rashwan AA (1988) Structural relationships between the southern and central parts of the Eastern Desert of Egypt: details of a fold and thrust belt. In: El Gaby S, Greiling RO (eds) The Pan-African Belt of Northeast Africa and adjacent areas. Vieweg and Sohn, Weisbaden, pp 121–145

Helmy HM, El Mahallawi MM (2003) Gabbro Akarem mafic-ultramafic complex, Eastern Desert, Egypt: a Late Precambrian analogue of Alaskan-type complex. Mineral Petrol 77:85–108

Irvine TN (1965) Chrome spinel as a petrogenetic indicator. Part I. Theory. Canad J Earth Sci 2:648–671

Ishii T, Robinson PT, Maekawa H, Fiske R (1992) Petrological studies of peridotites from diapiric Serpentinite Seamounts in the Izu-Ogasawara-Mariana forearc, leg 125. In: J Pearce, LB Stokking, et al. (eds) Proceedings of the Ocean Drilling Project, Leg 125, Scientific Results (College Station), pp 445–485.

Ishiwatari A, Sokolov SD, Vysotskiy SV (2003) Petrological diversity and origin of ophiolites in Japan and Far East Russia with emphasis on depleted harzburgite. In: Dilek Y, Robinson PT (eds) Ophiolites in Earth History. Geol Soc London Spec Pub 128:597–617

Jan MQ, Windley BF (1990) Chromian spinel-silicate chemistry in ultramafic rocks of the Jijal complex, Northwestern Pakistan. J Petrol 31:667–715

Johnson PR, Woldehaimanot B (2003) Development of the Arabian-Nubian Shield: Perspectives on accretion and deformation in the East African Orogen and the assembly of Gondwana. In: Yoshida M, Windley BF, Dasgupta S (eds) Proterozoic east gondwana: supercontinent assembly and breakup. Geol Soc London Spec Pub 289–325

Johnson PR, Kattan FH, Al-Saleh AM (2004) Neoproterozoic ophiolites in the Arabian Shield. In: Kusky TM (ed) Precambrian ophiolites and related rocks. In: Developments in precambrian geology 13, Elsevier, 129–162

Khalil AES, Azer MK (2007) Supra-subduction affinity in the Neoproterozoic serpentinites in the Eastern Desert, Egypt: Evidence from mineral composition. J Afr Earth Sci 49:136–152

Khudeir AA, El Haddad MA, Leake BE (1992) Compositional variation in chromite from the Eastern Desert. Mineral Mag 56:567–574

Klemm D, Klemm R, Murr A (2001) Gold of the Pharaohs – 6000 years of gold mining in Egypt and Nubia. J Afr Earth Sci 33:643–659

Kröner A, Greiling R, Reischmann T, Hussein IM, Stern RJ, Kruger J, Duur S, Zimmer M (1987) Pan-African crustal evolution in the Nubian segment of Northeast Africa. In: Kröner A (ed) Proterozoic Lithosphere Evolution. American Geophysical Union, Washington, DC, pp 235–257

Kröner A, Todt W, Hussein IM, Mansour M, Rashwan AA (1992) Dating of late Proterozoic ophiolites in Egypt and Sudan using the single grain zircon evaporation technique. Precamb Res 59:15–32

Kusky TM, Ramadan TM (2002) Structural controls on Neoproterozoic mineralization in the South Eastern Desert, Egypt: an integrated field, Landsat TM, and SIR-C/X SAR approach. J Afr Earth Sci 35:107–121

Loizenbauer J, Wallbrecher E, Fritz H, Neumayr P, Khudeir AA, Kloetzli U (2001) Structural geology, simple zircon ages and fluid inclusion studies of the Meatiq metamorphic core complex: Implications for Neoproterozoic tectonics in the Eastern Desert of Egypt. Precamb Res 110:357–383

Morishita T, Tani K, Shukuno H, Harigane Y, Tamura A, Kumagai H, Hellebrand E (2011) Diversity of melt conduits in the Izu-Bonin-Mariana forearc mantle: implications for the earliest stage of arc magmatism. Geology 39:411–414

Moussa EMM, Stern RJ, Manton WI, Ali KA (2008) SHRIMP zircon dating and Sm/Nd isotopic investigations of Neoproterozoic granitoids, Eastern Desert, Egypt. Precamb Res 160:341–356

Nassief MO, Macdonald R, Gass IG (1984) The Jebel Thurwah upper Proterozoic ophiolite complex, western Saudi Arabia. Geol Soc London 141:537–546

Noweir AM, Rashwan AA, Mehanna AM (2007) Genesis of the mafic-ultramafic and related metamorphic rocks in the northwestern part of Wadi Allaqi Terrain-south Eastern Desert, Egypt. Ann Geol Surv Egypt XXIX:51–75

Ohara Y, Stern RJ, Ishii T, Yurimoto H, Yamazaki T (2002) Peridotites from the Mariana Trough: first look at the mantle beneath an active back-arc basin. Contrib Mineral Petrol 143:1–18

Oweiss KhA, El Naggar AA, Abdel Razik KA, Moselhy N, Ali AB (2001) Gold exploration at Heianai area, South Eastern Desert, Egypt. Ann Geol Surv Egypt XXIV:435–450

Pallister JS, Stacey JS, Fischer LB, Premo WR (1988) Precambrian ophiolites of Arabia: Geologic settings, U-Pb geochronology, Pb-isotope characteristics, and implications for continental accretion. Precamb Res 38:1–54

Pearce JA (2003) Subduction zone ophiolites. In: Dilek Y, Newcomb S (eds) Ophiolite concept and the evolution of geological thought, GSA Special Paper 373, 269–294

Pearce JA, Lippard SJ, Roberts S (1984) Characteristics and tectonic significance of supra-subduction zone ophiolites. In: Kokelaar BP, Howells MF (eds) Marginal basin geology. Geol Soc Spec Publ 16:77–94

Price RC (1984) Late Precambrian Mafic-Ultramafic Complexes in Northeast Africa. Ph.D. thesis, Open University, Milton Keynes, 325.

Sack RO, Ghiorso MS (1991) Chromian spinels as petrogenetic indicators: thermodynamics and petrologic applications. Amer Mineral 76:827–847

Sadek MF, El-Ramly MF (1996) Geology, geochemistry and tectonic setting of the layered mafic ultramafic intrusions in Wadi Abu Fas, Wadi Um Domi area, south Eastern Desert, Egypt. Proc Geol Surv Cenn Conf 689–709

Shackleton RM (1994) Review of late Proterozoic sutures, ophiolitic me´langes and tectonics of eastern Egypt and north Sudan. Geol Rundsch 83:537–546

Shervais JW, Kimbrough DL, Renne PR, Hanan BB, Murchey B, Snow CA, Schuman MMZ, Beaman J (2004) Multi-stage origin of the coast range ophiolite. California; Implications for the life cycle of supra-subduction zone ophiolites. Inter Geol Rev 46:289–315

Sobolev NV, Logvinova AM (2005) Significance of accessory chrome spinels in identifying serpentinite paragenesis. Inter Geol Rev 47:58–64

Stern RJ (2002) Crustal evolution in the East African Orogen: a neodymium isotopic perspective. J Afr Earth Sci 34:109–117

Stern RJ (2004) Subduction initiation: spontaneous and induced. Earth Planet Sci Lett 226:275–292

Stern RJ, Gwinn CJ (1990) Origin of late precambrian intrusive carbonates, Eastern Desert of Egypt and Sudan: C, O, and Sr Isotopic Evidence. Precamb Res 46:259–272

Stern RJ, Hedge CE (1985) Geochronologic and isotopic constraints on Late Precambrian crustal evolution in the Eastern Desert of Egypt. Amer J Sci 285:97–127

Stern RJ, Nielsen KC, Best E, Sultan M, Arvidson RE, Kröner A (1990) Ophiolite Orientation of late Precambrian sutures in the Arabian-Nubian Shield. Geology 18:1103–1106

Stern RJ, Fouch MJ, Klemperer S (2003) An overview of the Izu-Bonin-Mariana Subduction Factory. In: Eiler J, Hirschmann M (eds) Inside the subduction factory, geophysical monograph 138, American Geophysical Union, 175–222

Stern RJ, Johnson PR, Kröner A, Yibas B (2004) Neoproterozoic ophiolites of the Arabian-Nubian Shield. In: Kusky TM (ed) Precambrian ophiolites and related rocks. Developments in Precambrian Geology 13:95–128

Taylor WEG, El Kazzaz YAH, Rashwan AA (1993) An outline of the tectonic framework for the Pan-African orogeny in the vicinity of Wadi Um Relan area, south Eastern Desert, Egypt. In: Thorweile U, Schandeimeier H (eds) Geoscientific research in northeast Africa, 31–34

Zimmer M, Kröner A, Jochum KP, Reischmann T, Todt W (1995) The Gabal Gerf complex: a Precambrian N-MORB ophiolite in the Nubian Shield, NE Africa. Chem Geol 123:29–51

Zoheir BA (2008) Characteristics and genesis of shear zone-related gold mineralization in Egypt: a case study from the Um El Tuyor mine, south Eastern Desert. Ore Geol Rev 34:445–470

Zoheir BA, Klemm DD (2007) The tectono-metamorphic evolution of the central part of the Neoproterozoic Allaqi-Heiani suture, south Eastern Desert of Egypt. Gond Res 12:289–304